

Review

Strain-Modulated Magnetism in MoS₂

Hongtao Ren ^{1,*} and Gang Xiang ^{2,*}

¹ School of Materials Science and Engineering, Liaocheng University, Hunan Road No. 1, Liaocheng 252000, China

² College of Physics, Sichuan University, Wangjiang Road No. 29, Chengdu 610064, China

* Correspondence: renhongtao@lcu.edu.cn (H.R.); gxiang@scu.edu.cn (G.X.)

Abstract: Since the experiments found that two-dimensional (2D) materials such as single-layer MoS₂ can withstand up to 20% strain, strain-modulated magnetism has gradually become an emerging research field. However, applying strain alone is difficult to modulate the magnetism of single-layer pristine MoS₂, but applying strain combined with other tuning techniques such as introducing defects makes it easier to produce and alter the magnetism in MoS₂. Here, we summarize the recent progress of strain-dependent magnetism in MoS₂. First, we review the progress in theoretical study. Then, we compare the experimental methods of applying strain and their effects on magnetism. Specifically, we emphasize the roles played by web buckles, which induce biaxial tensile strain conveniently. Despite some progress, the study of strain-dependent MoS₂ magnetism is still in its infancy, and a few potential directions for future research are discussed at the end. Overall, a broad and in-depth understanding of strain-tunable magnetism is very necessary, which will further drive the development of spintronics, straintronics, and flexible electronics.

Citation: Ren, H.; Xiang, G.

Strain-Modulated Magnetism in MoS₂. *Nanomaterials* **2022**, *12*, 1929.
<https://doi.org/10.3390/nano12111929>

Academic Editor: Antonio Di Bartolomeo

Received: 22 April 2022
Accepted: 1 June 2022
Published: 4 June 2022

Publisher's Note: MDPI stays neutral with regard to jurisdictional claims in published maps and institutional affiliations.



Copyright: © 2022 by the authors. Licensee MDPI, Basel, Switzerland. This article is an open access article distributed under the terms and conditions of the Creative Commons Attribution (CC BY) license (<https://creativecommons.org/licenses/by/4.0/>).

1. Introduction

Since Geim et al. [1] successfully peeled off stable monolayer graphene in 2004, 2D materials have gradually entered the vision of scientific researchers. While pristine graphene is diamagnetic, introducing defects and strains is an effective way to obtain long-range magnetic ordering [2–8]. Very recently, ferromagnetism (FM) has also been found in multilayer graphene [9], graphene nanoribbons [10], graphene open-shell nanostructures [11], twisted bilayer graphene [12–15], and graphene moiré superlattice [16]. Except for graphene, MoS₂ [17–21] has also attracted extensive attention. Interestingly, many experimental studies show that the defective MoS₂ nanostructures [18,19,22–47] also exhibit FM.

Notably, strain engineering [3–6,48–72] is also an effective way to mediate the magnetism of 2D materials. However, most of the previous work mainly focused on theoretical calculations. We have first introduced biaxial strain into the MoS₂ film through spontaneous buckling and found that biaxial strain can enhance its room-temperature FM (RTFM) [72–74]. As a whole, an extensive and in-depth understanding of strain-mediated magnetism in MoS₂ is needed, which would provide new avenues for spintronics and straintronics.

Here, we will give an overview of the timeline of strain-modulated magnetism in MoS₂ (Figure 1). We first review theoretical progress in various MoS₂ systems, such as nanoribbons (NRs) [17,48,49,51,75–82], hydrogenated [53,67] or nitrogen-doped [70,83] systems, defective systems [27,57,60,61,63,84–94] and 3d transition metal ion-doped systems [55,58,68,88,95–103]. Then, we outline the methods of introducing strain, such as using pre-stretched substrates [104,105], bending flexible substrates [106–114], utilizing lattice mismatch [115,116] or thermal mismatch [72,73,113,117–121], alloying [122],

creating buckles [72,73,104,105,114,121,123,124], using patterned substrates [125–130], bubbles [131–133], atomic force microscopy (AFM) tip [134,135], or piezoelectric stretching [136]. Among all the methods, creating buckles is suitable for detecting and studying the magnetism conveniently. Furthermore, we emphasize the roles played by web buckles, which induce biaxial tensile strain. Despite some progress, the study of strain-dependent MoS₂ magnetism is still in its infancy and a few potential directions for future research are discussed at the end.

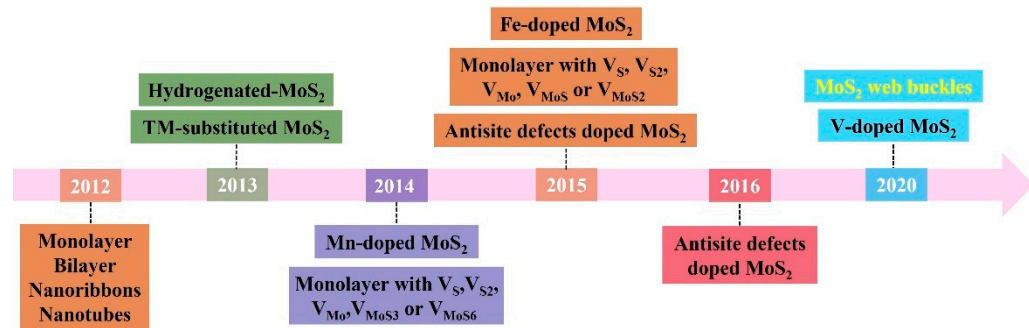


Figure 1. Timeline showing key developments of strain-modulated magnetism in MoS₂. Black font represents the theoretical progress; yellow font represents the experimental progress.

2. Progress in Theoretical Calculations of Strain-Mediated Magnetism

2.1. Nanoribbons

Similar to ZnO [80,137,138] and graphene [4,10] NRs with zigzag-terminated edges, zigzag MoS₂ NRs also exhibit FM [17,80] independent of NRs width and thickness due to the edge atoms. In contrast, armchair NRs show non-magnetism (NM). Interestingly, introducing adatoms can enhance the net magnetic moment of armchair NRs, but the FM of zigzag NRs is inhibited by the defects caused by adatoms [75]. Because the edge atoms are passivated, their spin polarization at the Fermi level is suppressed. Furthermore, an external static electric field can also reduce the energy gap of armchair NRs [76]. In detail, this electric field will drive metal-insulator phase transformation, which modulates or even suppresses FM.

In addition, monolayer and bilayer MoS₂ are also sensitive to tensile strain but cannot produce the long-range magnetic order in Figure 2. However, the magnetic moment in zigzag NRs is nearly doubled by 10% strain [51], as shown in Figure 2B, which may be related to the magnetic coupling from different edge atoms. As shown in Figure 2B–E, the variation is generally not monotonous [48,49,51].

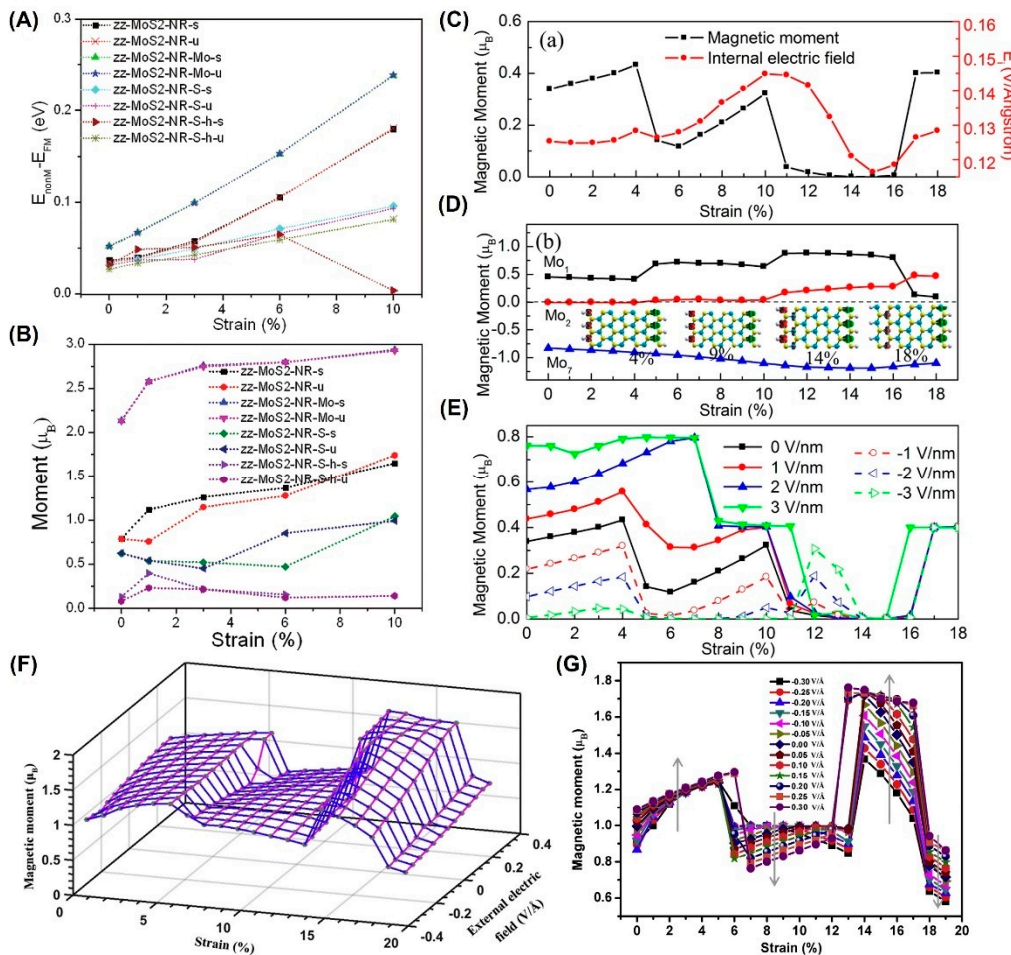


Figure 2. Strain-dependent magnetism in zigzag MoS₂ NRs. (A,B) Energy difference and magnetic moment of the zigzag nanoribbons under uniaxial tensile strain along its axis. (Reprinted/adapted with permission from Ref. [51]. Copyright 2012, American Chemical Society). (C) Tensile strain along -dependent magnetic moment of MoS₂ nanoribbons and the internal electric field across the edges of the ribbon (Reprinted/adapted with permission from Ref. [48]. Copyright 2012, American Chemical Society). (D) Magnetic moment on the edge Mo atoms versus strain. (Reprinted/adapted with permission from Ref. [48]. Copyright 2012, American Chemical Society). (E) Magnetic moment evolution of the strained MoS₂ nanoribbon under electric fields. (Reprinted/adapted with permission from Ref. [48]. Copyright 2012, American Chemical Society). (F) 3D view of the combined effects of strain and external electric field on magnetic moment. (Reprinted/adapted with permission from Ref. [81]. Copyright 2018, Elsevier). (G) Magnetic moment versus the strained nanoribbon with different external electric fields (Reprinted/adapted with permission from Ref. [81]. Copyright 2018, Elsevier).

Interestingly, applying tensile strain and an electric field in the zigzag direction can cause the reversible modulation of FM [48]. The applied strain is within the elastic limit of the material, which achieves the reversibility of regulation. Even for zigzag Janus MoSSe NRs, the magnetism shows a multi-stage change with the increase in strain, which is closely related to the electronic phase transition. After the electric field is applied again, the magnetism can be regulated more effectively [81].

However, this modulation is obviously different from that of the zigzag MoS₂ NRs shown in Figure 2E–G. Indeed, the difference in local spin density distribution determines the different modulation results of zigzag MoS₂ NRs and zigzag Janus MoSSe NRs.

2.2. Hydrogenated or Nitrogen-Doped Systems

Even after applying the biaxial tensile strain from about -8% to 8% , pristine monolayer and bilayer 2H-MoS₂ [49] are NM, indicating that no spin polarizations are aligned to form FM. However, other dichalcogenides materials, such as pristine VS₂ and VSe₂, exhibit FM [50], and the FM will increase rapidly when the strain increases from -5% to 5% . Metallic materials such as pristine 1T-MoS₂ [33,37,41,67,139,140], VS₂ [50,141,142] and VSe₂ [50,141–145] monolayer are more likely to form spontaneous magnetization.

In addition, the contribution of V atoms to magnetism is much greater than that of S or Se atoms [50]. In contrast, unstrained NbS₂ and NbSe₂ monolayers [52] are NM but can produce between 0.50 and $0.61 \mu_B$ per unit cell after applying 5% biaxial tensile strain. This novel magnetic behavior of NbS₂ and NbSe₂ monolayers is related not only to the bond length increased by strain but also to the metallic properties.

In fact, the self-exchange of populations between 4d orbitals of Nb atoms can lead to spin splitting [52,56]. Overall, V or Nb 4d states contribute mainly to the metallic state near the Fermi energy level [50,52,56]. By applying strain, the Curie temperature of the materials may be raised above room temperature [52], which will accelerate the spintronic application of 2D magnetic materials. However, MoS₂, WS₂, MoSe₂, and WSe₂ have no intrinsic magnetism [52] due to their characteristic band structures.

Hydrogen atoms [53,67] can modify the electronic structure of pristine 2H-MoS₂, but cannot produce spontaneous magnetism under $<3\%$ tensile strain [53], as shown in Figure 3A. With the increase in biaxial tensile strain, the magnetic moment and stability will be enhanced, as shown in Figure 3B. When the strain reaches 6.6% , the supercell obtains the most stable FM state, and the magnetic moment reaches $0.57 \mu_B$ per unit cell. In addition, its Curie temperature (T_c , $\sim 232\text{K}$) is much higher than that of the transition metal (TM)-doped system (T_c , $\sim 40\text{K}$) [84].

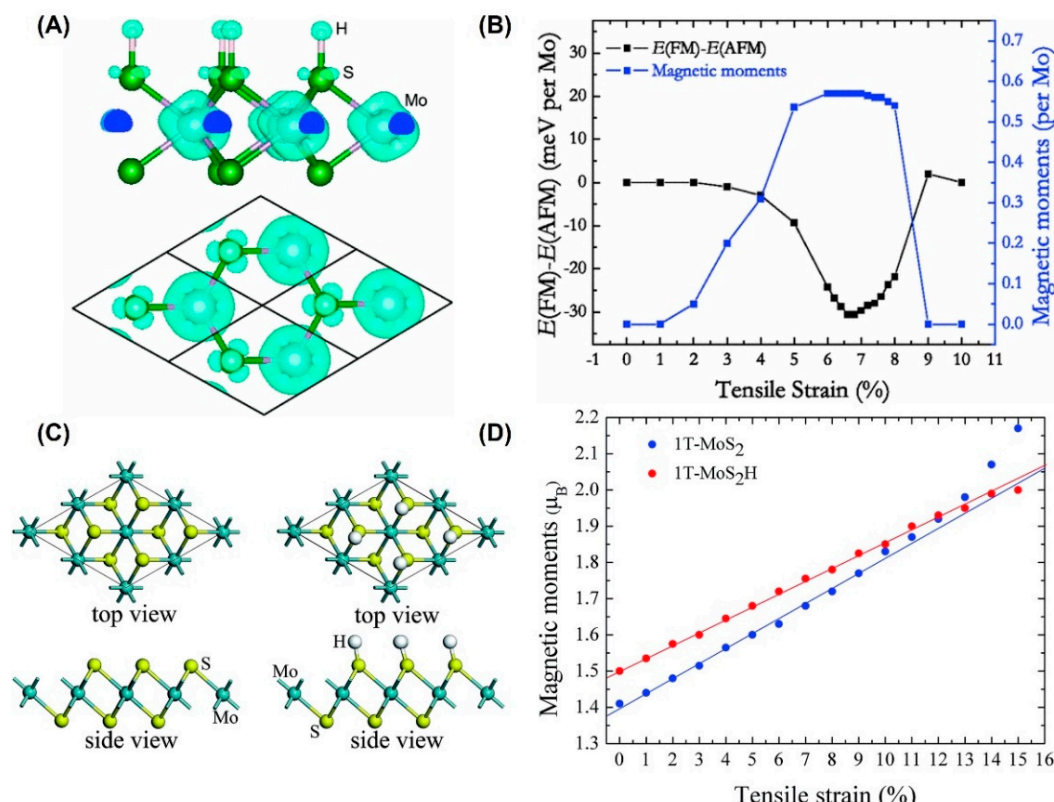


Figure 3. Strain-dependent magnetism in hydrogenated monolayer MoS₂. (A) Contour plots of the spin density of hydrogenated monolayer 2H-MoS₂ under the biaxial tensile strain of 6% . (Reprinted/adapted with permission from Ref. [53]. Copyright 2013, American Physical Society). (B) Energy difference per Mo atom for 2H-MoS₂H and the magnetic moment of Mo *d* orbitals per Mo atom versus Tensile Strain (%).

as a function of strain (Reprinted/adapted with permission from Ref. [53]. Copyright 2013, American Physical Society). (C) Monolayer 1T-MoS₂ model without and with hydrogen adsorption (Reprinted/adapted from Ref. [67] with permission from the Royal Society of Chemistry). (D) The function of magnetic moments of Mo atom in 1T-MoS₂ as tensile strain (Reprinted/adapted from Ref. [67] with permission from the Royal Society of Chemistry). Note that: The 2H phase structure with space group Pm2 has hexagonal symmetry and the primitive unit cell of the single-layer has three atoms. The S atom is with trigonal prismatic coordination around Mo atoms; The 1T phase is also with hexagonal symmetry and the primitive unit cell of the single-layer has three atoms. In the 1T phase with space group Pm1, the S atom is with octahedral coordination around Mo atoms.

However, 1T-MoS₂ and 1T-MoS₂H show FM behaviors, as shown in Figure 3C. Unlike 2H-MoS₂, the relationship between magnetic moments and strain is linear, as shown in Figure 3D [67]. The crystal field makes a great contribution to the magnetism of the system.

Similarly, the biaxial tensile strain can also modulate the magnetism of nitrogen-doped 2H-MoS₂ [70]. When the strain gradually increases to 17.09%, a single nitrogen doping structure (NM_{0.16}S₃₁) shows different magnetic phases. However, the magnetic moment of a dense nitrogen doping structure (NM_{0.4}S₇) steps from 0 up to 1 μ_B under 14% strain. In detail, unpaired electrons doped with nitrogen atoms will induce magnetic order. When the doped nitrogen atoms are too dense, the magnetic order will be weakened. However, the biaxial tensile strain has a good modulation effect on these two structures.

2.3. Defective Strained Systems

Inspired by the magnetism caused by conductive electrons in defective graphene. Many research groups tried to introduce single vacancies into the MoS₂ monolayer [57,94]. Experimentally, atomic single vacancies [91] (V_{Mo} : mono-molybdenum vacancy; V_S : mono-sulfur vacancy; V_{2S} : disulfur vacancy), vacancy complexes (V_{MoS3} : vacancy complex of Mo and nearby three sulfur; V_{MoS6} : vacancy complex of Mo nearby three disulfur pairs) and antisite defects [61,63] (S_{2Mo} : an S₂ column substituting a Mo atom; MoS : a Mo atom substituting an S column; Mo_{2S} : a Mo atom substituting an S₂ column) have been observed in CVD (chemical vapor deposition)-grown MoS₂ monolayer by atomic-resolution annular dark field (ADF) imaging on an aberration-corrected scanning transmission electron microscope (STEM) [86]. Through first-principles calculations shown in Table 1, it is found that pristine [60,94] and single vacancy [57,60,94]-MoS₂ monolayer are NM. Notably, when 19% biaxial tensile strain is applied to the pristine MoS₂ monolayer, 4×4 supercells produce a magnetic moment of 5 μ_B . However, the uniaxial strain cannot cause a magnetic phase transition regardless of the applied direction.

Table 1. Strain-dependent magnetism of single-layer MoS₂ with various defects.

System	Supercell Size	Maximum Strain	Magnetic Moment	Remarks
Pristine [94]	4 × 4	11%	0 μ_B	NM (0–11%), biaxial
Pristine [60]	4 × 4	20%	5 μ_B (19%)	NM (0–20%), biaxial
Pristine [60]	4 × 2 $\sqrt{3}$	20%	0 μ_B	NM (0–20%), x-axis
Pristine [60]	4 × 2 $\sqrt{3}$	20%	0 μ_B	NM (0–20%), y-axis
V_{Mo} [94]	4 × 4	11%	>2 μ_B (7–11%)	NM (<7%), biaxial
V_{Mo} [60]	4 × 4	20%	2.02 μ_B (14.5%)	NM (<6.5%), biaxial
V_{Mo} [60]	4 × 2 $\sqrt{3}$	20%	2.02 μ_B (7.5–20%)	NM (0–7.5%), x-axis
V_{Mo} [60]	4 × 2 $\sqrt{3}$	20%	2.02 μ_B (7.5–20%)	NM (0–7.5%), y-axis
V_S [57]	6 × 6	10%	2.0 μ_B (9%)	NM (<9%), biaxial
V_S [60]	4 × 4	20%	4.07 μ_B (14.5%)	NM (<8%), biaxial
V_S [60]	4 × 2 $\sqrt{3}$	20%	~2.07 μ_B (20%)	NM (0–15%), x-axis

V _S [60]	$4 \times 2\sqrt{3}$	20%	$\sim 2.0 \mu_B$ (15%)	NM (0–10%), y-axis
V _{S⁰} [91]	4×4	16%	$\sim 3 \mu_B$ (12%)	NM (0–10%), biaxial
V _{S¹⁺} [91]	4×4	16%	$2.0 \mu_B$ (12%)	NM (0–6%), biaxial
V _{S²⁺} [91]	4×4	16%	$2.0 \mu_B$ (12%)	NM (0%;6–8%), biaxial
V _{2S} [94]	4×4	11%	$>2 \mu_B$ (>10%)	NM (<10%), biaxial
V _{2S} [57]	6×6	10%	$5.5 \mu_B$ (9%)	NM (<9%), biaxial
V _{2S} [60]	4×4	22%	$7.45 \mu_B$ (13.5%)	NM (<9.5%), biaxial
V _{2S} [60]	$4 \times 2\sqrt{3}$	20%	$\sim 3.0 \mu_B$ (20%)	NM (0–15%), x-axis
V _{2S} [60]	$4 \times 2\sqrt{3}$	20%	$\sim 1.0 \mu_B$ (20%)	NM (0–15%), y-axis
V _{MoS} [60]	4×4	20%	$4.04 \mu_B$ (13%)	NM (<5.5%), biaxial
V _{MoS} [60]	$4 \times 2\sqrt{3}$	20%	$\sim 1.7 \mu_B$ (10%); $0 \mu_B$	NM (<10%, 15%), x-axis y-axis
V _{MoS} [60]	$4 \times 2\sqrt{3}$	20%	$\sim 5.9 \mu_B$ (20%)	$\sim 2 \mu_B$ (<5%), biaxial
V _{MoS₂} [60]	$4 \times 2\sqrt{3}$	20%	$0 \mu_B$	NM (>4%), x-axis
V _{MoS₂} [60]	$4 \times 2\sqrt{3}$	20%	$\sim 2 \mu_B$ (0–20%)	y-axis
V _{MoS₃} [57]	6×6	10%	$4.0 \mu_B$ (10%)	NM (<10%), biaxial
V _{MoS₆} [57]	6×6	-12%	$12.0 \mu_B$ (9%)	NM (-12%), biaxial
S _{2Mo} [61]	6×6	8%	$2.0 \mu_B$ (8%)	NM (<8%), biaxial
MoS ₂ [61]	6×6	8%	$2.0 \mu_B$ (8%)	NM (<8%), biaxial
Mos [63]	4×4	7%	$2.0 \mu_B$ (-7–4%)	NM (5–7%), biaxial

Interestingly, unstrained MoS₂ monolayers with V_{Mo} [60,94], V_S [57,60], V_{2S} [57,60,94], V_{MoS} [60], V_{MoS₃} [57], S_{2Mo} [61] and Mos₂ [61] are NM, as shown in Figure 4, while unstrained MoS₂ monolayers with V_{MoS₂} [46,60,146], V_{MoS₆} [57] and Mos [63] are magnetic. In detail, the charge transfer and Mo atoms around the defects contribute mainly to magnetism. Furthermore, spin reorientation and the largest magnetic moment occur in the V_{2S}-MoS₂ monolayer [60], as shown in Figure 4A,B, which is related to magneto-crystalline anisotropy. With the increase in the tensile strain, FM-NM-FM phase transformation has been observed in V_S-MoS₂. Li et al. [91] have also drawn the magnetic phase diagram caused by strain and external electric field, as shown in Figure 4C,D. After applying strain, the charge sulfur vacancy defect shows rich magnetic responses.

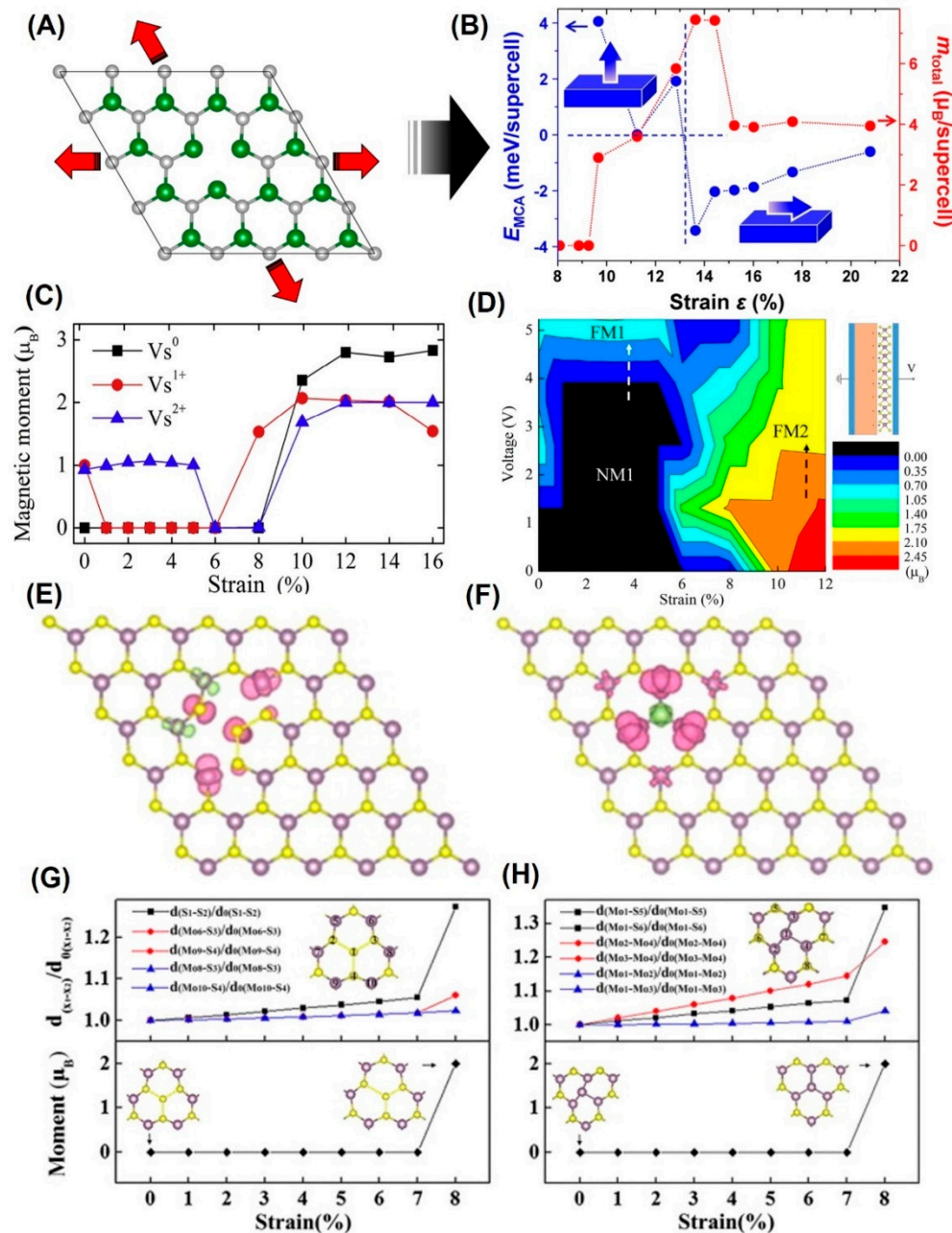


Figure 4. (A) Schematic illustration of MoS₂ ML with V_{2s} under biaxial tensile strain (Reprinted/adapted with permission from Ref. [60]. Copyright 2013, American Physical Society). (B) EMCA and magnetic moment vs. applied tensile strain. (Reprinted/adapted with permission from Ref. [60]. Copyright 2013, American Physical Society). (C) The magnetic moments of Vs-MoS₂ under strain with charge state $q = 0, 1, 2$. (Reprinted/adapted with permission from Ref. [91]. Copyright 2018, Elsevier). (D) The magnetic phase diagram of Vs-MoS₂ driven by strain and voltage with a capacitor structure. (Reprinted/adapted with permission from Ref. [91]. Copyright 2018, Elsevier). (E,F) Spin density distributions of MoS₂ systems with S_{2Mo} and MoS₂ under 8% strains. (Reprinted/adapted with permission from Ref. [61]. Copyright 2015, Elsevier). (G,H) The evolutions of magnetic moments of the supercell and the parameter d/d_0 with the strain for the Vs and V_{2s}. (Reprinted/adapted with permission from Ref. [61]. Copyright 2015, Elsevier).

Since Zhou et al. [86] and Jin et al. [147] found the antisite defects in the MoS₂ monolayer by STEM imaging in 2013, researchers have been trying to understand their magnetic characteristics in Figure 4E–H. In detail, the defect is an intrinsic structural defect. After applying 8% biaxial tensile strain, the system will produce long-range magnetic order [61]. Overall, the spin density is mainly distributed in the sulfur atom and

its nearest or second neighbor, the Mo atom. However, the antisite-doped monolayer exhibits a high spin state under the biaxial strain from −7% to 4%. With the further increase in tensile strain, magnetism will vanish. The position of the antisite atom is related to the magnetism of the system. In addition, it is found that strained Vs can greatly improve the hydrogen evolution activity of MoS₂ basal planes [148]. The sulfur vacancy will become a new active site and tune the adsorption-free energy of the hydrogen atom.

2.4. 3d Transition Metal (TM) Ion-Doped Systems

Doping engineering [149–157] is a traditional way to control the properties of materials, especially for 2D materials. Recently, it has been confirmed experimentally [149,150,158–162] that 3d TM doping can induce ferromagnetism in nonmagnetic MoS₂, which can be combined with strain engineering to tune the magnetism, as shown in Table 2.

Table 2. Strain-dependent magnetism of TM-doped single-layer MoS₂.

Dopant	Supercell Size	Maximum Strain	Magnetic Moment/ μ_B	Remarks
V [88]	5 × 5	20%	0 μ_B (−20–20%)	
V [100]	4 × 4	5%	0.81 μ_B (0%)	AFM (3% or −2%)
Mn [88]	5 × 5	20%	1.0 μ_B (0%)	0 (−20%); 2.8 μ_B (20%)
Mn [55]	4 × 4	6%	1.0 (1%)	3.0 μ_B (6%), biaxial
Mn [98]	4 × 4	−10%	1.0 (−10–9%)	be almost independent on the size of supercell, no matter under a tensile or compressive strain
Mn [98]	5 × 5	−10%	1.0 (−10–9%)	
Mn [98]	6 × 6	−10%	1.0 (−10–9%)	
Mn [98]	Unit cell	9%	1.0 μ_B (0–3%)	3.0 μ_B (4–9%), biaxial
Fe [88]	5 × 5	20%	2.0 μ_B (0%)	0 (−20%); 4.2 μ_B (20%)
Fe [58]	4 × 4	6%	2.04 μ_B (0%)	4.0 μ_B (3.5–6%), spin reorientation
Fe [68]	Unit cell	9%	2.0 μ_B (0–5%)	4.0 μ_B (6–9%), biaxial
Co [88]	5 × 5	20%	5.0 μ_B (15%)	0 (−20%); 3.3 μ_B (20%)
Co [68]	Unit cell	9%	3.0 μ_B (0–7%)	3.4 μ_B (8%), biaxial
Ni [88]	5 × 5	20%	5.0 μ_B (10%)	0 (−20%); 2.0 μ_B (20%)
Ni [68]	Unit cell	9%	4.0 μ_B (0–8%)	3.7 μ_B (9%), biaxial
Cu [88]	5 × 5	20%	5.0 μ_B (0%)	0 (−20%); 0 μ_B (20%)
Zn [88]	5 × 5	20%	3.0 μ_B (10%)	0 (−20%); 0 μ_B (20%)
Cr [88]	5 × 5	20%	0 μ_B (−20–20%)	
Ti [88]	5 × 5	20%	0 μ_B (−20–20%)	
Sc [88]	5 × 5	20%	0 μ_B (−20–20%)	

Interestingly, TM-doped systems show different magnetic responses. Except for V, Cr, Ti, and Sc atoms [88], the TM-doped systems without strain are nonmagnetic, and no matter how much biaxial strain is applied, there will be no long-range magnetic order. Arguably, Ma et al. [100] reported that V-doped monolayer MoS₂ exhibits magnetic half-metal at zero strain. After 2% compressive strain or 3% tensile strain is applied, the system will change from an FM state to an antiferromagnetic state.

Notably, the magnetic properties of Co/Ni/Cu/Zn-doped molybdenum disulfide show nonlinear changes with strain. After applying 20% compressive strain, the system is nonmagnetic. When the applied tensile strain reaches a specific value, the system will obtain a high spin state (5 μ_B for the Co-doped; 5 μ_B for the Ni-doped; 5 μ_B for the Cu-doped; 3 μ_B for the Zn-doped). However, the magnetic moment will reduce to 0 under 20% tensile strain, except for the Co-doped system (3 μ_B).

The linear monotonicity of magnetism with strain has also been found in Mn-doped and Fe-doped MoS₂ systems, which is similar to those of 1T-MoS₂ and 1T-MoS₂H. In detail,

the systems are NM under a 20% compressive strain. Applying 20% tensile strain, the systems have obtained high spin states ($2.8 \mu_B$ for Mn-doped; $4.3 \mu_B$ for Fe-doped).

In general, strain engineering is an effective method to control the magnetism of the TM-doped molybdenum disulfide system.

3. Experimental Progress of Strain-Mediated Magnetism

3.1. Methods of Applying Strain

Since the experiments revealed that 2D materials can withstand up to 20% strain, strain-modulated magnetism has gradually become an emerging research field. However, it is difficult to apply strain directly in suspended 2D materials in Table 3.

Table 3. The range and types in strained MoS₂ systems by different inducing methods. HOPG: highly oriented pyrolytic graphite; PMN-PT: [Pb(Mg_{1/3}Nb_{2/3})O₃]_{0.7}·[PbTiO₃]_{0.3}. δ_{mem} : the deflection of the membrane.

Methods	Substrates	Layers	Ranges	Remarks
Pre-stretches substrate	Gel-film [104]	3–5 L	0.2–2.5%	Uniaxial tensile
Pre-stretches substrate	PDMS [105]	2–10 L	20% (PDMS)	Uniaxial
Flexible substrate	Polycarbonate [106]	1–2 L	0–2.2%	Uniaxial tensile
Flexible substrate	Polymer [107]	1, few	0–0.8%	Uniaxial tensile
Flexible substrate	Ag-coated PET [108]	20–80 nm	0–0.02%	Uniaxial tensile
Flexible substrate	PET [109]	1 L	−0.7–0.7%	Uniaxial
Flexible substrate	PVA [110]	1 L	0–1.49%	Uniaxial tensile
Flexible substrate	Polyimide [111]	1–2 L	0–0.32%	Uniaxial tensile
Flexible substrate	Polyimide [112]	2 L	0–1.19%	biaxial
Flexible substrate	PDMS [113]	1 L	0–4.8%	Uniaxial tensile
Flexible substrate	PDMS [114]	2–10 L	~2.2%	Uniaxial tensile
Lattice mismatch	Si/SiO ₂ [115]	1 L	~1.24%	Intrinsic tensile
Lattice mismatch	HOPG [116]	1 L	~1.76%	Anisotropic tensile
Thermal mismatch	Si/SiO ₂ [113]	1 L	~1.0%	Intrinsic tensile
Thermal mismatch	Si/SiO ₂ [117]	1 L	0.4%; 0.6%	Intrinsic tensile
Thermal mismatch	Si/SiO ₂ [118]	1 L	~0.76%	Intrinsic tensile
Thermal mismatch	Si/SiO ₂ [119]	2 L	~0.34%;	Intrinsic compressive
Thermal mismatch	Sapphire [117]	1 L	0.15%; 0.2%	Intrinsic tensile
Thermal mismatch	<i>h</i> -BN [117]	1 L	~0.8%; ~0.2%	Intrinsic tensile
Thermal mismatch	Mica [117]	1 L	~0.8%; ~0.2%	Intrinsic tensile
Thermal mismatch	PDMS [120]	1 L	<–0.2%	Biaxial compressive
Thermal mismatch	Al ₂ O ₃ [72,73]	~60 nm	−0.29–−0.45%	Biaxial compressive
Thermal mismatch	m-quartz [121]	1 L	~−0.776%	Uniaxial compressive
Alloying	MoS _{2x} Se _{2(1-x)} [122]	1 L	<4%	Biaxial tensile
Creating buckles	Gel-film [104]	3–5 L	0.2–2.5%	Uniaxial tensile
Creating buckles	PDMS [114]	2–10 L	~2.2%	Uniaxial
Creating buckles	PDMS [105]	2–10 L	~1–~2%	Uniaxial compressive
Creating buckles	Al ₂ O ₃ [72,73]	~60 nm	−0.45–−1.7%	Biaxial
Creating buckles	m-quartz [121]	1 L	0.14–1.58%	Uniaxial tensile
Creating buckles	Au films [123]	1 L	−1.16–−2.04%	Uniaxial
Creating buckles	Si/SiO ₂ [124]	10–21 nm	0.32–1.11%	Uniaxial tensile
Patterned substrate	Holey Si ₃ N ₄ [125]	2 L	~1.8%	Biaxial tensile
Patterned substrate	Rippled Si/SiO ₂ [126]	4 L	~0.5%	Uniaxial tensile
Patterned substrate	SiO ₂ nanocones [127]	1 L	~0.565%	Biaxial tensile
Patterned substrate	SiO ₂ nanopillars [128]	1 L	~2%	Uniaxial tensile
Patterned substrate	Cone-Al ₂ O ₃ [129]	2 L	~0.04%	Tensile/compressive

Patterned substrate	Pyramid-Al ₂ O ₃ [129]	2 L	~0.05%	Tensile/compressive
Patterned substrate	ZnO rods [130]	1 L	0~0.6%	Periodic biaxial
Bubbles	PDMS [131]	1, few	2.9~3.5%	Biaxial tensile
Bubbles	<i>h</i> -BN [132]	1 L	~2%	Gradient tensile
Bubbles	Si/SiO ₂ cavity [133]	multi-	~0.8~1.5%	Biaxial, >5.6%
AFM tip	Si/SiO ₂ [134]	1~3 L	δ_{mem} : ~33 nm	Isotropic
AFM tip	Si/SiO ₂ [135]	1 L	4.7×10^{-5} F	Isotropic
Piezoelectric substrate	PMN-PT [136]	3 L	0~0.2%	Biaxial compressive

In 2013, Andres et al. [104] created wrinkles in few-layer MoS₂ by pre-stretching the gel-film substrate, resulting in uniaxial tensile strain up to 2.5%. In the same year, uniaxial tensile strain (0~2.2%) was also applied in the MoS₂/polycarbonate system by using four-point bending equipment [106]. Since then, many research groups have tried to apply strain through a variety of flexible substrates, including polymers [107], polyethyleneterephthalate (PET) [108,109], polyvinyl alcohol (PVA) [110], polyimide (PI) [111,112] and polydimethylsiloxane (PDMS) [113,114].

In addition, the researchers have found that the intrinsic tensile strain (0.15~1.37%) was also introduced in CVD grown-monolayer MoS₂ [113,115,117~119,122]. This intrinsic tensile strain is caused by the mismatch of thermal expansion coefficients [72,73,113,115~117,121]. Interestingly, whether through flexible substrate [104] or thermal mismatch [72,73], the strain state of MoS₂ materials can be further mediated by creating buckles [72,73,104,105,114,121,123,124].

Recently, it has also been experimentally found that the strain can be introduced into the materials through patterned substrates such as holey Si₃N₄ [125], rippled Si/SiO₂ [126], SiO₂ nanocones [127], SiO₂ nanopillars [128], pyramid/cones Al₂O₃ [129], ZnO nanorods arrays [130], nanodots arrays, and so on. During the transfer of MoS₂ samples, bubbles [131~133] are often formed to introduce large strains into the samples. Notably, most of the methods required additional equipment to provide external stimulation, such as an AFM tip [134,135], an electromechanical device [74], or a focused laser beam [136]. Because scanning superconducting quantum interference device (SQUID) needs to be conducted in a cryogenic temperature and vibration environment, it is difficult to detect the strained material system. So far, material systems that can spontaneously form buckles [72~74] are more suitable for magnetic study.

3.2. Spontaneous Formation of Web Buckles

Spontaneous buckling [163,164] is frequently observed in the film system of traditional materials. When the residual strain in the film reaches its critical value, it will drive the film to delamination from the substrate and from spontaneous wrinkles [72~74]. Interfacial adhesion [73,165] is one of the key factors in determining whether buckling is formed or not. Relatively low adhesion is conducive to the formation and propagation of buckles. Because there is no hanging bond on the surface of 2D materials such as MoS₂, the van der Waals (vdW) force is the interaction between the material and the substrate, and its interface adhesion is relatively low. Since then, MoS₂ films are very likely to become the perfect platform for understanding the phenomena of spontaneous buckling [73].

Recently, our group prepared ultra-smooth MoS₂ films [72,73] by polymer-assisted deposition (PAD), as shown in Figure 5. When the thickness of the film is about 400 nm, its roughness is about 1 nm. In the laboratory environment, MoS₂ films will also spontaneously form buckles due to external disturbance. Inspired by this experimental observation, we have used a tungsten probe close to the touch film to apply a point load. Once the probe touches the film, web buckles will be formed and further spread to the whole film surface. The formed large-area film with web buckles is very suitable for the

SQUID test. Surprisingly, there is no obvious damage to the web buckle's structure after the magnetic test.

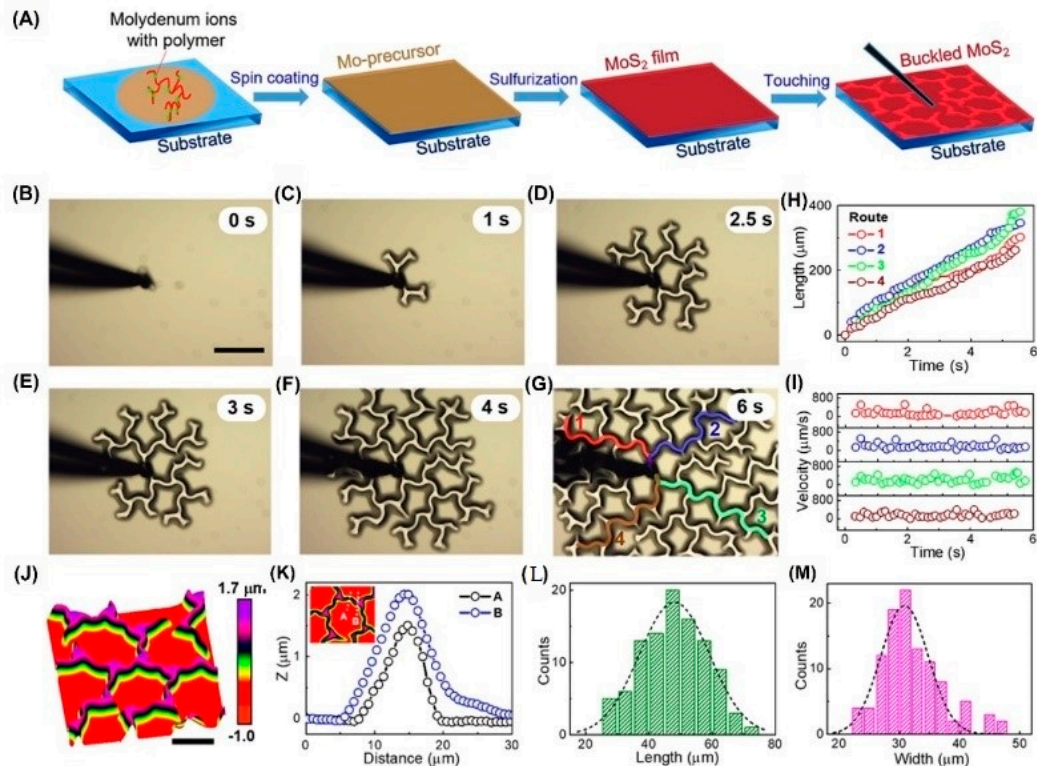


Figure 5. Formation of large-area web buckles. **(A)** Schematic illustration of the growth of a MoS₂ thin film with PAD and the triggering of buckles by a probe touching. **(B–G)** In situ observation of large area web buckles formed on an as-grown MoS₂ thin film with a thickness of 370 nm. Scale bar, 100 μm . **(H,I)** Propagating distances and velocities of buckles along four different branches as labeled in **(G)**, as a function of time, respectively. **(J)** AFM 3D topography of a buckled MoS₂ thin film with a thickness of 230 nm. Scale bar, 20 μm . **(K)** Two height-profile lines crossing the middle of a telephone cord (line A) and a node position (line B) as shown in the inset. **(L,M)** Statistical histograms of lengths and widths of buckles. Reprinted/adapted with permission from Ref. [73]. Copyright 2019, American Chemical Society.

3.3. Web Buckle-Mediated RTFM

Strain engineering [6,49,51,52,56–58,61,72,73,166] is a straightforward way to mediate the magnetism of MoS₂. However, most of the previous work [48–53,55,57,58,60,61,63,67,68,70,81,88,90,91,94,97,98,100] mainly focused on theoretical calculations. In the experiment, it was very difficult to apply biaxial strain directly to 2D materials. In order to clarify the strain-mediated FM in MoS₂, the following problems must be solved: (1) how to quantitatively determine the strain in the system experimentally; (2) how to select two suitable strain states to study their ferromagnetism; (3) how to measure ferromagnetism in different zones of web buckles.

Since Ferrari et al. [167] successfully measured the uniaxial and biaxial strain in graphene samples in 2009, Raman spectroscopy has become a powerful tool to characterize the strain deformation of two-dimensional materials. Soon after 2013, the strain-tunable energy gap was studied in mono-, bi-, and tri-layer MoS₂ [104,106,136,168,169]. Notably, Yagmurcukardes et al. [170] studied how the strain modulated the Raman characteristics of single-layer materials by first-principle calculation. Therefore, we used Raman spectroscopy to quantify the strain in web buckles (Figure 6) [72–74]. In detail, it is estimated by Raman mapping that about 68% of the region in the flat film has strain variations.

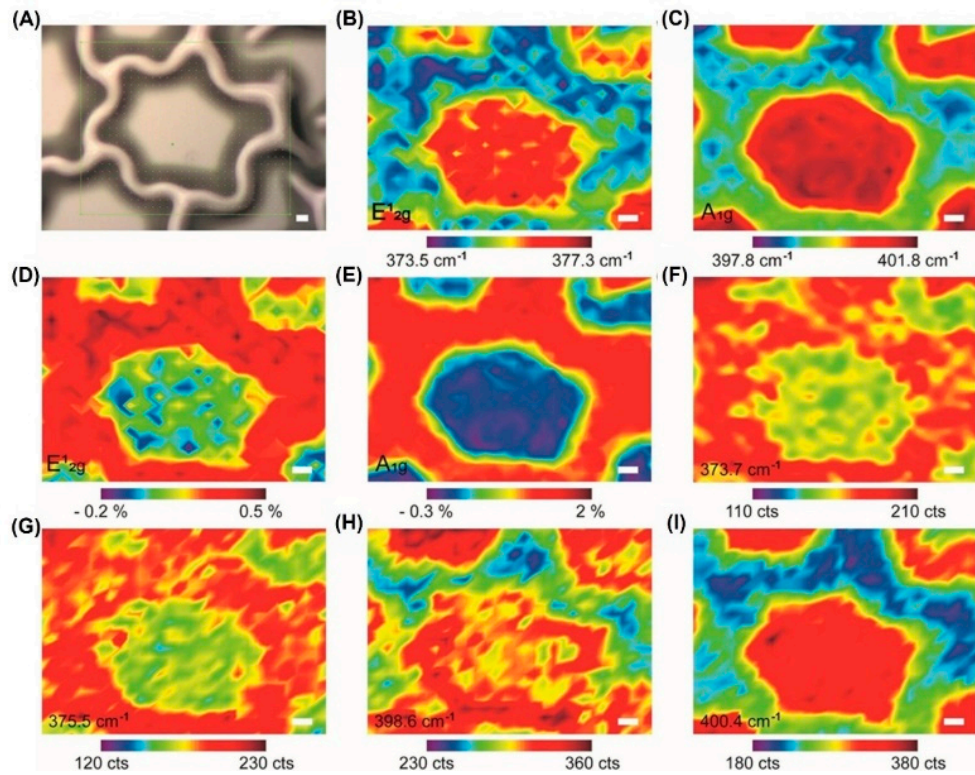


Figure 6. Native strain variations in MoS₂ web buckles. **(A)** Optical image of MoS₂ web buckles. **(B,C)** Raman position mapping in the E¹_{2g} and A_{1g} modes. **(D,E)** Strain mapping of MoS₂ web buckles is estimated by the response of Raman-active modes to the applied biaxial strain for single-layer MoS₂. **(F–I)** Raman intensity mapping in E¹_{2g} (between 373.7 cm⁻¹ and 375.5 cm⁻¹) and A_{1g} (between 398.6 cm⁻¹ and 400.4 cm⁻¹). Scale bars: 5 μm. (Reprinted/adapted with permission from Ref. [72]. Copyright 2020, American Institute of Physics).

In order to clarify the strain-dependent ferromagnetism, we selected flat films and buckled films to test, as shown in Figure 7. After buckling, the saturation magnetization at 300K increases to 7.5 times that before buckling. This is because the biaxial tensile strain induced by web buckles produces the generation of more defects such as Vs. The enhancement of magnetism may be related to the decrease in compressive strain and the increase in defects.

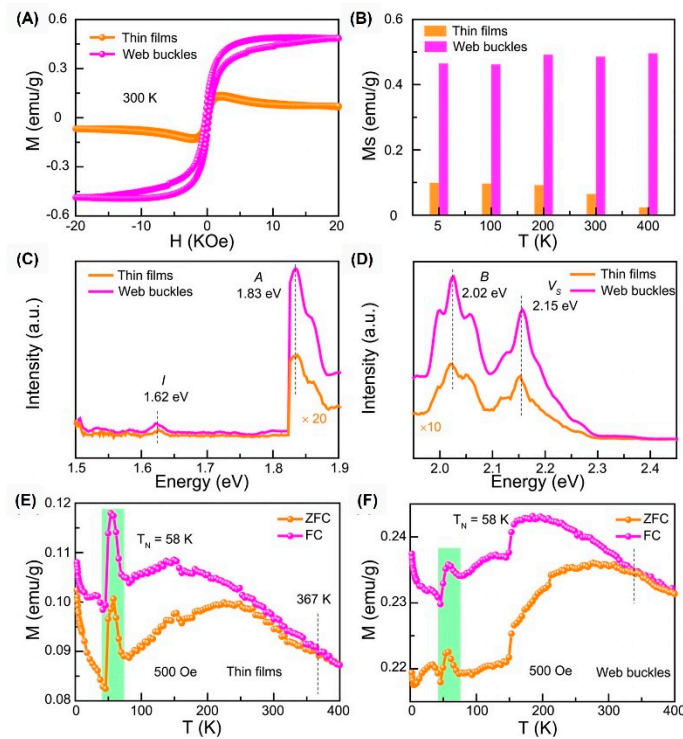


Figure 7. Ferromagnetism of MoS_2 thin films and web buckles. (A) M - H curves (A), M_s - T (B), FL excitation spectra (C), and FL emission spectra (D) of MoS_2 thin films and web buckles. (E,F) M - T of MoS_2 thin films and web buckles. (Reprinted/adapted with permission from Ref. [72]. Copyright 2020, American Institute of Physics).

So far, we cannot distinguish the magnetism from different buckled areas. Although traditional magnetic force microscopy can be obtained, we believe that there are too many impurity signals to identify the information in the samples. Hopefully, the newly emerging magnetic imaging technologies will provide technical support for further research.

4. Conclusions and Outlook

In this review, we have summarized the recent developments in strain-dependent magnetism in MoS_2 . First, we reviewed the progress of the theoretical study. Then, we compared the experimental methods of introducing strain and their effects on the ferromagnetism. We emphasized the roles played by web buckles since they could induce biaxial tensile strain conveniently for further tests, including magnetic measurements. Obviously, despite some progress, the study of strain-dependent MoS_2 magnetism is still in its infancy.

Although RTFM has been enhanced experimentally by biaxial strain [72] induced by web buckles, the magnetism contributions from different zones cannot be distinguished experimentally. Since most conventional magnetic probes [171] require the sample area to be at the millimeter level, magnetic testing of the micron wrinkled area is a great challenge. Very recently, magnetic imaging techniques have emerged as important tools for investigating 2D materials, such as magnetic force microscopy (MFM) [172–178], SQUID [179,180], magneto-optical Kerr effect (MOKE) [181,182] and scanning nitrogen-vacancy center microscopy (SNVM) [183–187]. These techniques make it possible to detect the magnetism of the wrinkled area.

Since the modulation effect of uniaxial strain on the properties of materials is weaker than that of biaxial strain, whether the RTFM of molybdenum disulfide can be regulated by uniaxial strain has always been a mystery, which is worthy of further exploration. In addition, the substrates commonly used in experiments are isotropic, so it is relatively

easy to introduce isotropic strain (such as biaxial strain) into 2D materials. Recently, anisotropic substrates such as *m*-quartz [121,188] have been used in experiments, which provides a new idea for introducing uniaxial strain into MoS₂. We believe that the regulation of uniaxial strain on FM can be explained clearly by combining nanoscale magnetic detection instruments.

Overall, an extensive and in-depth understanding of strain-mediated magnetism in MoS₂ is needed, which would provide new avenues for spintronics [189–197] and straintronics [198–202].

Author Contributions: Writing—original draft preparation, H.R.; writing—review and editing, H.R. and G.X.; supervision, G.X. All authors have read and agreed to the published version of the manuscript.

Funding: This research was funded by National Natural Science Foundation of China (Grant No. 52172272), Shandong Province Natural Science Foundation (Grant No. ZR202103040767), and Doctoral Scientific Research Foundation of Liaocheng University (Grant No. 318052054).

Institutional Review Board Statement: Not applicable.

Informed Consent Statement: Not applicable.

Data Availability Statement: Not applicable.

Conflicts of Interest: The authors declare no conflict of interest.

References

1. Novoselov, K.S.; Geim, A.K.; Morozov, S.V.; Jiang, D.; Zhang, Y.; Dubonos, S.V.; Grigorieva, I.V.; Firsov, A.A. Electric field effect in atomically thin carbon films. *Science* **2004**, *306*, 666.
2. Yazyev, O.V. Emergence of magnetism in graphene materials and nanostructures. *Rep. Prog. Phys.* **2010**, *73*, 056501. <http://dx.doi.org/10.1088/0034-4885/73/5/056501>.
3. Huang, B.; Yu, J.; Wei, S.H. Strain control of magnetism in graphene decorated by transition-metal atoms. *Phys. Rev. B* **2011**, *84*, 075415. <https://doi.org/10.1103/physrevb.84.075415>.
4. Kou, L.; Tang, C.; Guo, W.; Chen, C. Tunable magnetism in strained graphene with topological line defect. *ACS Nano* **2011**, *5*, 1012–1017.
5. Ma, Y.; Dai, Y.; Guo, M.; Niu, C.; Yu, L.; Huang, B. Strain-induced magnetic transitions in half-fluorinated single layers of BN, GaN and graphene. *Nanoscale* **2011**, *3*, 2301–2306. <https://doi.org/10.1039/c4nr01961j>.
6. Santos, E.J.G.; Ayuela, A.; Sanchez-Portal, D. Strain-tunable spin moment in Ni-doped graphene. *J. Phys. Chem. C* **2012**, *116*, 1174–1178. <https://doi.org/10.1021/jp2077374>.
7. Santos, E.J.G.; Ayuela, A.; Fagan, S.B.; Mendes Filho, J.; Azevedo, D.L.; Souza Filho, A.G.; Sánchez-Portal, D. Switching on magnetism in Ni-doped graphene: Density functional calculations. *Phys. Rev. B* **2008**, *78*, 195420. <https://doi.org/10.1103/physrevb.78.195420>.
8. Boukhvalov, D.W.; Katsnelson, M.I. sp-electron magnetic clusters with a large spin in graphene. *ACS Nano* **2011**, *5*, 2440–2446.
9. Swain, A.K.; Bahadur, D. Deconvolution of mixed magnetism in multilayer graphene. *Appl. Phys. Lett.* **2014**, *104*, 242413. <https://doi.org/10.1063/1.4884426>.
10. Magda, G.Z.; Jin, X.; Hagymási, I.; Vancsó, P.; Osváth, Z.; Nemes-Incze, P.; Hwang, C.; Biró, L.P.; Tapasztó, L. Room - temperature magnetic order on zigzag edges of narrow graphene nanoribbons. *Nature* **2014**, *514*, 608.
11. Li, J.; Sanz, S.; Corso, M.; Choi, D.J.; Peña, D.; Frederiksen, T.; Pascual, J.I. Single spin localization and manipulation in graphene open-shell nanostructures. *Nat. Commun.* **2019**, *10*, 200.
12. Sharpe, A.L.; Fox, E.J.; Barnard, A.W.; Finney, J.; Watanabe, K.; Taniguchi, T.; Kastner, M.A.; Goldhaber-Gordon, D. Emergent ferromagnetism near three-quarters filling in twisted bilayer graphene. *Science* **2019**, *365*, 605–608.
13. Lu, X.; Stepanov, P.; Yang, W.; Xie, M.; Aamir, M.A.; Das, I.; Urgell, C.; Watanabe, K.; Taniguchi, T.; Zhang, G.; et al. Superconductors, orbital magnets and correlated states in magic-angle bilayer graphene. *Nature* **2019**, *574*, 653–657.
14. Liu, X.; Hao, Z.; Khalaf, E.; Lee, J.Y.; Ronen, Y.; Yoo, H.; Haei Najafabadi, D.; Watanabe, K.; Taniguchi, T.; Vishwanath, A.; et al. Tunable spin-polarized correlated states in twisted double bilayer graphene. *Nature* **2020**, *583*, 221–225.
15. Zhou, H.; Holleis, L.; Saito, Y.; Cohen, L.; Huynh, W.; Patterson Caitlin, L.; Yang, F.; Taniguchi, T.; Watanabe, K.; Young, A.F. Isospin magnetism and spin-polarized superconductivity in bernal bilayer graphene. *Science* **2022**, *375*, 774–778.
16. Chen, G.; Sharpe, A.L.; Fox, E.J.; Zhang, Y.-H.; Wang, S.; Jiang, L.; Lyu, B.; Li, H.; Watanabe, K.; Taniguchi, T.; et al. Tunable correlated Chern insulator and ferromagnetism in a moiré superlattice. *Nature* **2020**, *579*, 56–61.
17. Li, Y.; Zhou, Z.; Zhang, S.; Chen, Z. MoS₂ nanoribbons: high stability and unusual electronic and magnetic properties. *J. Am. Chem. Soc.* **2008**, *130*, 16739–16744.

18. Jaglicic, Z.; Jeromen, A.; Trontelj, Z.; Mihailovic, D.; Arcon, D.; Remskar, M.; Mrzel, A.; Dominko, R.; Gaberscek, M.; Martinez-Agudo, J.M.; et al. Magnetic properties of MoS₂ nanotubes doped with lithium. *Polyhedron* **2003**, *22*, 2293–2295.
19. Mihailovic, D.; Jaglicic, Z.; Arcon, D.; Mrzel, A.; Zorko, A.; Remskar, M.; Kabanov, V.V.; Dominko, R.; Gaberscek, M.; Gómez-García, C.J.; et al. Unusual magnetic state in Lithium-doped MoS₂ nanotubes. *Phys. Rev. Lett.* **2003**, *90*, 146401, <https://doi.org/10.1103/PhysRevLett.90.146401>.
20. Vojvodic, A.; Hinnemann, B.; Nørskov, J.K. Magnetic edge states in MoS₂ characterized using density-functional theory. *Phys. Rev. B* **2009**, *80*, 125416, <https://doi.org/10.1103/PhysRevB.80.125416>.
21. Shidpour, R.; Manteghian, M. A density functional study of strong local magnetism creation on MoS₂ nanoribbon by sulfur vacancy. *Nanoscale* **2010**, *2*, 1429–1435.
22. Gao, D.; Shi, S.; Tao, K.; Xia, B.; Xue, D. Tunable ferromagnetic ordering in MoS₂ nanosheets with fluorine adsorption. *Nanoscale* **2015**, *7*, 4211–4216.
23. Chacko, L.; Swetha, A.K.; Anjana, R.; Jayaraj, M.K.; Aneesh, P.M. Wasp-waisted magnetism in hydrothermally grown MoS₂ nanoflakes. *Mater. Res. Express.* **2016**, *3*, 116102.
24. Gao, G.H.; Chen, C.; Xie, X.B.; Su, Y.T.; Kang, S.D.; Zhu, G.C.; Gao, D.Y.; Trampert, A.; Cai, L.T. Toward edges-rich MoS₂ layers via chemical liquid exfoliation triggering distinctive magnetism. *Mater. Res. Lett.* **2017**, *5*, 267–275.
25. Kondo, G.; Yokoyama, N.; Yamada, S.; Hashimoto, Y.; Ohata, C.; Katsumoto, S.; Haruyama, J. Edge-spin-derived magnetism in few-layer MoS₂ nanomeshes. *AIP. Adv.* **2017**, *7*, 125019.
26. Zhengong, M.; Cheuk-Lam, H.; Guijun, L.; Sheung-Mei, N.; Hon-Fai, W.; Chi-Wah, L.; Wai-Yeung, W. Edge decoration of MoS₂ monolayer with ferromagnetic CoFe nanoparticles. *Mater. Res. Express.* **2018**, *5*, 115010.
27. Zhou, Q.; Su, S.; Cheng, P.; Hu, X.; Zeng, M.; Gao, X.; Zhang, Z.; Liu, J.-M. Robust ferromagnetism in zigzag-edge rich MoS₂ pyramids. *Nanoscale* **2018**, *10*, 11578–11584.
28. Kaur, N.; Mir, R.A.; Pandey, O.P. A novel study on soft ferromagnetic nature of nano molybdenum sulphide (MoS₂). *Physica B* **2019**, *574*, 411684.
29. Sarma, S.; Ghosh, B.; Ray, S.C.; Wang, H.T.; Mahule, T.S.; Pong, W.F. Electronic structure and magnetic behaviors of exfoliated MoS₂ nanosheets. *J. Phys. Condens. Matter* **2019**, *31*, 135501.
30. Sanikop, R.; Sudakar, C. Tailoring magnetically active defect sites in MoS₂ nanosheets for spintronics applications. *ACS Appl. Nano Mater.* **2020**, *3*, 576.
31. Sun, B.; Li, Q.L.; Chen, P. Room-temperature ferromagnetism of single-crystalline MoS₂ nanowires. *IET Micro Nano Lett.* **2014**, *9*, 468–470.
32. Zhang, R.; Li, Y.; Qi, J.; Gao, D. Ferromagnetism in ultrathin MoS₂ nanosheets: from amorphous to crystalline. *Nanoscale Res. Lett.* **2014**, *9*, 586.
33. Cai, L.; He, J.F.; Liu, Q.H.; Yao, T.; Chen, L.; Yan, W.S.; Hu, F.C.; Jiang, Y.; Zhao, Y.D.; Hu, T.D.; et al. Vacancy-induced ferromagnetism of MoS₂ nanosheets. *J. Am. Chem. Soc.* **2015**, *137*, 2622–2627.
34. Martinez, L.M.; Delgado, J.A.; Saiz, C.L.; Cosio, A.; Wu, Y.; Villagrán, D.; Gandha, K.; Karthik, C.; Nlebedim, I.C.; Singamaneni, S.R. Magnetic and electrocatalytic properties of transition metal doped MoS₂ nanocrystals. *J. Appl. Phys.* **2018**, *124*, 153903.
35. Tsai, S. P.; Yang, C. Y.; Lee, C. J.; Lu, L. S.; Liang, H. L.; Lin, J. X.; Yu, Y. H.; Chen, C. C.; Chung, T. K.; Kaun, C. C.; Hsu, H. S.; Huang, S. Y.; Chang, W. H.; He, L. C.; Lai, C. H.; Wang, K. L. Room-temperature ferromagnetism of single-layer MoS₂ induced by antiferromagnetic proximity of yttrium iron garnet. *Adv. Quantum Technol.* **2021**, *4*, 2000104.
36. Gao, D.; Si, M.; Li, J.; Zhang, J.; Zhang, Z.; Yang, Z.; Xue, D. Ferromagnetism in freestanding MoS₂ nanosheets. *Nanoscale Res. Lett.* **2013**, *8*, 129.
37. Yan, S.M.; Qiao, W.; He, X.M.; Guo, X.B.; Xi, L.; Zhong, W.; Du, Y.W. Enhancement of magnetism by structural phase transition in MoS₂. *Appl. Phys. Lett.* **2015**, *106*, 012408.
38. Park, C.-S.; Chu, D.; Shon, Y.; Lee, J.; Kim, E.K. Room temperature ferromagnetic and ambipolar behaviors of MoS₂ doped by manganese oxide using an electrochemical method. *Appl. Phys. Lett.* **2017**, *110*, 222104.
39. Yang, Z.; Gao, D.; Zhang, J.; Xu, Q.; Shi, S.; Tao, K.; Xue, D. Realization of high curie temperature ferromagnetism in atomically thin MoS₂ and WS₂ nanosheets with uniform and flower-like morphology. *Nanoscale* **2015**, *7*, 650–658.
40. Kumar, A.; Pawar, S.; Sharma, S.; Kaur, D. Bipolar resistive switching behavior in MoS₂ nanosheets fabricated on ferromagnetic shape memory alloy. *Appl. Phys. Lett.* **2018**, *112*, 262106.
41. Xia, B.R.; Liu, P.T.; Liu, Y.G.; Gao, D.Q.; Xue, D.S.; Ding, J. Re doping induced 2H-1T phase transformation and ferromagnetism in MoS₂ nanosheets. *Appl. Phys. Lett.* **2018**, *113*, 013101.
42. Shirokura, T.; Muneta, I.; Kakushima, K.; Tsutsui, K.; Wakabayashi, H. Strong edge-induced ferromagnetism in sputtered MoS₂ film treated by post-annealing. *Appl. Phys. Lett.* **2019**, *115*, 192404.
43. Duan, H.; Li, G.; Tan, H.; Wang, C.; Li, Q.; Liu, C.; Yin, Y.; Li, X.; Qi, Z.; Yan, W. Sulfur-vacancy-tunable interlayer magnetic coupling in centimeter-scale MoS₂ bilayer. *Nano Res.* **2022**, *15*, 881–888.
44. Mathew, S.; Gopinadhan, K.; Chan, T.K.; Yu, X.J.; Zhan, D.; Cao, L.; Rusydi, A.; Breese, M.B.H.; Dhar, S.; Shen, Z.X.; et al. Magnetism in MoS₂ induced by proton irradiation. *Appl. Phys. Lett.* **2012**, *101*, 102103.
45. Tongay, S.; Varnoosfaderani, S.S.; Appleton, B.R.; Wu, J.; Hebard, A.F. Magnetic properties of MoS₂: existence of ferromagnetism. *Appl. Phys. Lett.* **2012**, *101*, 123105.
46. Han, S.W.; Hwang, Y.H.; Kim, S.H.; Yun, W.S.; Lee, J.D.; Park, M.G.; Ryu, S.; Park, J.S.; Yoo, D.H.; Yoon, S.P.; et al. Controlling ferromagnetic easy axis in a layered MoS₂ single crystal. *Phys. Rev. Lett.* **2013**, *110*, 247201.

47. Wang, Y.; Tseng, L.-T.; Murmu, P.P.; Bao, N.; Kennedy, J.; Ionescu, M.; Ding, J.; Suzuki, K.; Li, S.; Yi, J. Defects engineering induced room temperature ferromagnetism in transition metal doped MoS₂. *Mater. Design.* **2017**, *121*, 77–84.
48. Kou, L.; Tang, C.; Zhang, Y.; Heine, T.; Chen, C.; Frauenheim, T. Tuning magnetism and electronic phase transitions by strain and electric field in zigzag MoS₂ nanoribbons. *J. Phys. Chem. Lett.* **2012**, *3*, 2934–2941.
49. Lu, P.; Wu, X.J.; Guo, W.L.; Zeng, X.C. Strain-dependent electronic and magnetic properties of MoS₂ monolayer, bilayer, nanoribbons and nanotubes. *Phys. Chem. Chem. Phys.* **2012**, *14*, 13035–13040.
50. Ma, Y.D.; Dai, Y.; Guo, M.; Niu, C.W.; Zhu, Y.T.; Huang, B.B. Evidence of the existence of magnetism in pristine VX₂ monolayers (X = S, Se) and their strain-induced tunable magnetic properties. *ACS Nano* **2012**, *6*, 1695–1701.
51. Pan, H.; Zhang, Y.W. Tuning the electronic and magnetic properties of MoS₂ nanoribbons by strain engineering. *J. Phys. Chem. C* **2012**, *116*, 11752–11757.
52. Zhou, Y.G.; Wang, Z.G.; Yang, P.; Zu, X.T.; Yang, L.; Sun, X.; Gao, F. Tensile strain switched ferromagnetism in layered NbS₂ and NbSe₂. *ACS Nano* **2012**, *6*, 9727–9736.
53. Shi, H.; Pan, H.; Zhang, Y.-W.; Yakobson, B.I. Strong ferromagnetism in hydrogenated monolayer MoS₂ tuned by strain. *Phys. Rev. B* **2013**, *88*, 205305.
54. Guo, H.; Lu, N.; Wang, L.; Wu, X.; Zeng, X.C. Tuning electronic and magnetic properties of early transition-metal dichalcogenides via tensile strain. *J. Phys. Chem. C* **2014**, *118*, 7242–7249.
55. Qi, J.S.; Li, X.; Chen, X.F.; Hu, K.G. Strain tuning of magnetism in Mn doped MoS₂ monolayer. *J. Phys. Condens. Matter* **2014**, *26*, 256003.
56. Xu, Y.; Liu, X.; Guo, W. Tensile strain induced switching of magnetic states in NbSe₂ and NbS₂ single layers. *Nanoscale* **2014**, *6*, 12929–12933.
57. Zheng, H.L.; Yang, B.S.; Wang, D.D.; Han, R.L.; Du, X.B.; Yan, Y. Tuning magnetism of monolayer MoS₂ by doping vacancy and applying strain. *Appl. Phys. Lett.* **2014**, *104*, 132403.
58. Chen, Z.P.; He, J.J.; Zhou, P.; Na, J.; Sun, L.Z. Strain control of the electronic structures, magnetic states, and magnetic anisotropy of Fe doped single-layer MoS₂. *Comp. Mater. Sci.* **2015**, *110*, 102–108.
59. Manchanda, P.; Sharma, V.; Yu, H.B.; Sellmyer, D.J.; Skomski, R. Magnetism of Ta dichalcogenide monolayers tuned by strain and hydrogenation. *Appl. Phys. Lett.* **2015**, *107*, 032402.
60. Yun, W.S.; Lee, J.D. Strain-induced magnetism in single-layer MoS₂: origin and manipulation. *J. Phys. Chem. C* **2015**, *119*, 2822–2827.
61. Zheng, H.L.; Yang, B.S.; Wang, H.X.; Chen, Z.Y.; Yan, Y. Strain induced modulation to the magnetism of antisite defects doped monolayer MoS₂. *J. Magn. Magn. Mater.* **2015**, *386*, 155–160.
62. Chen, P.; Zhao, X.; Wang, T.X.; Dai, X.Q.; Xia, C.X. Electronic and magnetic properties of Ag-doped monolayer WS₂ by stain. *J. Alloy. Compd.* **2016**, *680*, 659–664.
63. Sahoo, M.P.K.; Wang, J.; Zhang, Y.J.; Shimada, T.; Kitamura, T. Modulation of gas adsorption and magnetic properties of monolayer-MoS₂ by antisite defect and strain. *J. Phys. Chem. C* **2016**, *120*, 14113–14121.
64. Yang, Y.; Fan, X.L.; Zhang, H. Effect of strain on the magnetic states of transition-metal atoms doped monolayer WS₂. *Comp. Mater. Sci.* **2016**, *117*, 354–360.
65. Zhang, W.; Guo, H.T.; Jiang, J.; Tao, Q.C.; Song, X.J.; Li, H.; Huang, J. Magnetism and magnetocrystalline anisotropy in single-layer PtSe₂: Interplay between strain and vacancy. *J. Appl. Phys.* **2016**, *120*, 013904.
66. Luo, M.; Shen, Y.H. Effect of strain on magnetic coupling in Ga-doped WS₂ monolayer: Ab initio study. *J. Supercond. Nov. Magn.* **2018**, *31*, 1801–1805.
67. Xu, W.; Yan, S.M.; Qiao, W. Magnetism in monolayer 1T-MoS₂ and 1T-MoS₂H tuned by strain. *RSC Adv.* **2018**, *8*, 8435–8441.
68. Zhu, Y.; Liang, X.; Qin, J.; Deng, L.; Bi, L. Strain tunable magnetic properties of 3d transition-metal ion doped monolayer MoS₂: A first-principles study. *AIP Adv.* **2018**, *8*, 055917.
69. Cortés, N.; Ávalos-Ovando, O.; Rosales, L.; Orellana, P.A.; Ulloa, S.E. Tunable Spin-Polarized Edge Currents in Proximity-Induced Transition Metal Dichalcogenides. *Phys. Rev. Lett.* **2019**, *122*, 086401.
70. Nie, S.; Li, Z. Strain effect on the magnetism of N-doped molybdenum disulfide. *Phys. Status Solidi B* **2019**, *256*, 1900110.
71. Yang, S.; Chen, Y.; Jiang, C. Strain engineering of two-dimensional materials: Methods, properties, and applications. *InfoMat* **2021**, *3*, 397–420.
72. Ren, H.T.; Zhang, L.; Xiang, G. Web buckle-mediated room-temperature ferromagnetism in strained MoS₂ thin films. *Appl. Phys. Lett.* **2020**, *116*, 012401.
73. Ren, H.T.; Xiong, Z.X.; Wang, E.Z.; Yuan, Z.Q.; Sun, Y.F.; Zhu, K.L.; Wang, B.L.; Wang, X.W.; Ding, H.Y.; Liu, P.; et al. Watching dynamic self-assembly of web buckles in strained MoS₂ thin films. *ACS Nano* **2019**, *13*, 3106–3116.
74. Ren, H.T.; Xiang, G.; Lu, J.T.; Zhang, X.; Zhang, L. Biaxial strain-mediated room temperature ferromagnetism of ReS₂ web buckles. *Adv. Electron. Mater.* **2019**, *5*, 1900814.
75. Ataca, C.; Sahin, H.; Akturk, E.; Ciraci, S. Mechanical and electronic properties of MoS₂ nanoribbons and their defects. *J. Phys. Chem. C* **2011**, *115*, 3934–3941.
76. Dolui, K.; Das Pemmaraju, C.; Sanvito, S. Electric field effects on armchair MoS₂ nanoribbons. *ACS Nano* **2012**, *6*, 4823–4834.
77. Pan, H.; Zhang, Y.W. Edge-dependent structural, electronic and magnetic properties of MoS₂ nanoribbons. *J. Mater. Chem.* **2012**, *22*, 7280–7290.
78. Wen, Y.N.; Gao, P.F.; Chen, X.; Xia, M.G.; Zhang, Y.; Zhang, S.L. Width-dependent structural stability and magnetic properties of monolayer zigzag MoS₂ nanoribbons. *Mod. Phys. Lett. B* **2017**, *31*, 1750017.

79. Chen, K.Y.; Deng, J.K.; Ding, X.D.; Sun, J.; Yang, S.; Liu, J.Z. Ferromagnetism of 1T'-MoS₂ nanoribbons stabilized by edge reconstruction and its periodic variation on nanoribbons width. *J. Am. Chem. Soc.* **2018**, *140*, 16206–16212.
80. Liu, Y.C.; Ren, H.T.; Gao, P.F.; Zhang, Y.; Xia, M.G.; Zhang, S.L. Flexible modulation of electronic and magnetic properties of zigzag H-MoS₂ nanoribbons by crack defects. *J. Phys. Condens. Matter* **2018**, *30*, 285302.
81. Wang, M.; Pang, Y.; Liu, D.Y.; Zheng, S.H.; Song, Q.L. Tuning magnetism by strain and external electric field in zigzag Janus MoSSe nanoribbons. *Comp. Mater. Sci.* **2018**, *146*, 240–247.
82. Vancso, P.; Hagymasi, I.; Castenetto, P.; Lambin, P. Stability of edge magnetism against disorder in zigzag MoS₂ nanoribbons. *Phys. Rev. Mater.* **2019**, *3*, 094003.
83. Chen, M.Y.; Hu, C.; Luo, X.F.; Hong, A.J.; Yu, T.; Yuan, C.L. Ferromagnetic behaviors in monolayer MoS₂ introduced by nitrogen-doping. *Appl. Phys. Lett.* **2020**, *116*, 073102.
84. Cheng, Y.C.; Zhu, Z.Y.; Mi, W.B.; Guo, Z.B.; Schwingenschlogl, U. Prediction of two-dimensional diluted magnetic semiconductors: Doped monolayer MoS₂ systems. *Phys. Rev. B* **2013**, *87*, 100401.
85. Najmaei, S.; Liu, Z.; Zhou, W.; Zou, X.L.; Shi, G.; Lei, S.D.; Yakobson, B.I.; Idrobo, J.C.; Ajayan, P.M.; Lou, J. Vapour phase growth and grain boundary structure of molybdenum disulphide atomic layers. *Nat. Mater.* **2013**, *12*, 754–759.
86. Zhou, W.; Zou, X.; Najmaei, S.; Liu, Z.; Shi, Y.; Kong, J.; Lou, J.; Ajayan, P.M.; Yakobson, B.I.; Idrobo, J.C. Intrinsic structural defects in monolayer molybdenum disulfide. *Nano Lett.* **2013**, *13*, 2615–2622.
87. Zhou, Y.; Yang, P.; Zu, H.; Gao, F.; Zu, X. Electronic structures and magnetic properties of MoS₂ nanostructures: atomic defects, nanoholes, nanodots and antidots. *Phys. Chem. Chem. Phys.* **2013**, *15*, 10385–10394.
88. Zhou, Y.G.; Su, Q.L.; Wang, Z.G.; Deng, H.Q.; Zu, X.T. Controlling magnetism of MoS₂ sheets by embedding transition-metal atoms and applying strain. *Phys. Chem. Chem. Phys.* **2013**, *15*, 18464–18470.
89. Najmaei, S.; Yuan, J.T.; Zhang, J.; Ajayan, P.; Lou, J. Synthesis and defect investigation of two-dimensional molybdenum disulfide atomic layers. *Acc. Chem. Res.* **2015**, *48*, 31–40.
90. Zhang, H.; Fan, L.; Yang, Y.; Xiao, P. Strain engineering the magnetic states of vacancy-doped monolayer MoSe₂. *J. Alloy. Compd.* **2015**, *635*, 307–313.
91. Li, A.; Pan, J.; Yang, Z.; Zhou, L.; Xiong, X.; Ouyang, F. Charge and strain induced magnetism in monolayer MoS₂ with S vacancy. *J. Magn. Magn. Mater.* **2018**, *451*, 520–525.
92. Yang, H.P.; Ouyang, W.G.; Yan, X.X.; Li, Z.C.; Yu, R.; Yuan, W.J.; Luo, J.; Zhu, J. Bilayer MoS₂ quantum dots with tunable magnetism and spin. *AIP Adv.* **2018**, *8*, 115103.
93. Bouarissa, A.; Layadi, A.; Maghraoui-Meherzi, H. Experimental study of the diamagnetism and the ferromagnetism in MoS₂ thin films. *Appl. Phys. A* **2020**, *126*, 93.
94. Tao, P.; Guo, H.; Yang, T.; Zhang, Z. Strain-induced magnetism in MoS₂ monolayer with defects. *J. Appl. Phys.* **2014**, *115*, 054305.
95. Kang, K.; Fu, S.C.; Shayan, K.; Anthony, Y.; Dadras, S.; Yuzan, X.; Kazunori, F.; Terrones, M.; Zhang, W.; Stefan, S.; Meunier, V.; Vamivakas, A.N.; Yang, E.H. The effects of substitutional Fe-doping on magnetism in MoS₂ and WS₂ monolayers. *Nanotechnology* **2021**, *32*, 095708.
96. Zhao, C.Y.; Jin, C.H.; Wu, J.L.; Ji, W. Magnetism in molybdenum disulphide monolayer with sulfur substituted by 3d transition metals. *J. Appl. Phys.* **2016**, *120*, 144305.
97. Li, H.X.; Huang, M.; Cao, G.Y. Magnetic properties of atomic 3d transition-metal chains on S-vacancy-line templates of monolayer MoS₂: effects of substrate and strain. *J. Mater. Chem. C* **2017**, *5*, 4557–4564.
98. Miao, Y.P.; Huang, Y.H.; Bao, H.W.; Xu, K.W.; Ma, F.; Chu, P.K. Tunable magnetic coupling in Mn-doped monolayer MoS₂ under lattice strain. *J. Phys. Condens. Matter* **2018**, *30*, 215801.
99. Zhang, S.F.; Li, Z.Q.; Li, J.; Hao, G.L.; He, C.Y.; Ouyang, T.; Zhang, C.X.; Tang, C.; Zhong, J.X. Strain effects on magnetic states of monolayer MoS₂ doped with group IIIA to VA atoms. *Physica E* **2019**, *114*, 113609.
100. Miao, Y.P.; Bao, H.W.; Fan, W.; Ma, F. Modulation of the electronic structure and magnetism performance of V-doped monolayer MoS₂ by strain engineering. *J. Phys. Chem. Solids* **2020**, *142*, 109459.
101. Yue, Y.L.; Jiang, C.; Han, Y.L.; Wang, M.; Ren, J.; Wu, Y.K. Magnetic anisotropies of Mn-, Fe-, and Co-doped monolayer MoS₂. *J. Magn. Magn. Mater.* **2020**, *496*, 165929.
102. Gao, B.; Huang, C.; Zhu, F.; Ma, C.L.; Zhu, Y. Magnetic properties of Mn-doped monolayer MoS₂. *Phys. Lett. A* **2021**, *414*, 127636.
103. Han, X.P.; Benkraouda, M.; Amrane, N. S vacancy enhanced ferromagnetism in Mn-doped monolayer MoS₂: A hybrid functional study. *Chem. Phys.* **2021**, *541*, 111043.
104. Castellanos-Gomez, A.; Roldan, R.; Cappelluti, E.; Buscema, M.; Guinea, F.; van der Zant, H.S.J.; Steele, G.A. Local strain engineering in atomically thin MoS₂. *Nano Lett.* **2013**, *13*, 5361–5366.
105. Iguliniz, N.; Frisenda, R.; Bratschitsch, R.; Castellanos-Gomez, A. Revisiting the buckling metrology method to determine the Young's modulus of 2D materials. *Adv. Mater.* **2019**, *31*, 1807150.
106. Conley, H.J.; Wang, B.; Ziegler, J.I.; Haglund, R.F.; Pantelides, S.T.; Bolotin, K.I. Bandgap engineering of strained monolayer and bilayer MoS₂. *Nano Lett.* **2013**, *13*, 3626–3630.
107. Rice, C.; Young, R.J.; Zan, R.; Bangert, U.; Wolverson, D.; Georgiou, T.; Jalil, R.; Novoselov, K.S. Raman-scattering measurements and first-principles calculations of strain-induced phonon shifts in monolayer MoS₂. *Phys. Rev. B* **2013**, *87*, 081307.
108. Lee, J.H.; Jang, W.S.; Han, S.W.; Baik, H.K. Efficient hydrogen evolution by mechanically strained MoS₂ nanosheets. *Langmuir* **2014**, *30*, 9866–9873.

109. Pak, S.; Lee, J.; Lee, Y.W.; Jang, A.R.; Ahn, S.; Ma, K.Y.; Cho, Y.; Hong, J.; Lee, S.; Jeong, H.Y.; et al. Strain-mediated interlayer coupling effects on the excitonic behaviors in an epitaxially grown MoS₂/WS₂ van der Waals heterobilayer. *Nano Lett.* **2017**, *17*, 5634–5640.
110. Li, Z.; Lv, Y.; Ren, L.; Li, J.; Kong, L.; Zeng, Y.; Tao, Q.; Wu, R.; Ma, H.; Zhao, B.; et al. Efficient strain modulation of 2D materials via polymer encapsulation. *Nat. Commun.* **2020**, *11*, 1151.
111. John, A.P.; Thenapparambil, A.; Thalakulam, M. Strain-engineering the Schottky barrier and electrical transport on MoS₂. *Nanotechnology* **2020**, *31*, 275703.
112. Thai, K.Y.; Park, I.; Kim, B.J.; Hoang, A.T.; Na, Y.; Park, C.U.; Chae, Y.; Ahn, J.-H. MoS₂/Graphene photodetector array with strain-modulated photoresponse up to the near-infrared regime. *ACS Nano* **2021**, *15*, 12836–12846.
113. Liu, Z.; Amani, M.; Najmaei, S.; Xu, Q.; Zou, X.; Zhou, W.; Yu, T.; Qiu, C.; Birdwell, A.G.; Crowne, F.J.; et al. Strain and structure heterogeneity in MoS₂ atomic layers grown by chemical vapour deposition. *Nat. Commun.* **2014**, *5*, 5246.
114. Brennan, C.J.; Nguyen, J.; Yu, E.T.; Lu, N.S. Interface adhesion between 2D materials and elastomers measured by buckle delaminations. *Adv. Mater. Interfaces* **2015**, *2*, 1500176.
115. Amani, M.; Chin, M.L.; Mazzoni, A.L.; Burke, R.A.; Najmaei, S.; Ajayan, P.M.; Lou, J.; Dubey, M. Growth-substrate induced performance degradation in chemically synthesized monolayer MoS₂ field effect transistors. *Appl. Phys. Lett.* **2014**, *104*, 203506.
116. Zhang, C.; Li, M.-Y.; Tersoff, J.; Han, Y.; Su, Y.; Li, L.-J.; Muller, D.A.; Shih, C.-K. Strain distributions and their influence on electronic structures of WSe₂–MoS₂ laterally strained heterojunctions. *Nat. Nanotechnol.* **2018**, *13*, 152–158.
117. Chae, W.H.; Cain, J.D.; Hanson, E.D.; Murthy, A.A.; Dravid, V.P. Substrate-induced strain and charge doping in CVD-grown monolayer MoS₂. *Appl. Phys. Lett.* **2017**, *111*, 143106.
118. Luo, S.W.; Cullen, C.P.; Guo, G.C.; Zhong, J.X.; Duesberg, G.S. Investigation of growth-induced strain in monolayer MoS₂ grown by chemical vapor deposition. *Appl. Surf. Sci.* **2020**, *508*, 145127.
119. Yu, Y.; Jung, G.S.; Liu, C.; Lin, Y.-C.; Rouleau, C.M.; Yoon, M.; Eres, G.; Duscher, G.; Xiao, K.; Irle, S.; et al. Strain-induced growth of twisted bilayers during the coalescence of monolayer MoS₂ crystals. *ACS Nano* **2021**, *15*, 4504–4517.
120. Plechinger, G.; Castellanos-Gomez, A.; Buscema, M.; van der Zant, H.S.J.; Steele, G.A.; Kuc, A.; Heine, T.; Schüller, C.; Korn, T. Control of biaxial strain in single-layer molybdenite using local thermal expansion of the substrate. *2D Mater.* **2015**, *2*, 015006.
121. Wang, J.; Han, M.; Wang, Q.; Ji, Y.; Zhang, X.; Shi, R.; Wu, Z.; Zhang, L.; Amini, A.; Guo, L.; et al. Strained epitaxy of monolayer transition metal dichalcogenides for wrinkle arrays. *ACS Nano* **2021**, *15*, 6633–6644.
122. Taghinejad, H.; Eftekhar, A.A.; Campbell, P.M.; Beatty, B.; Taghinejad, M.; Zhou, Y.; Perini, C.J.; Moradinejad, H.; Henderson, W.E.; Woods, E.V.; et al. Strain relaxation via formation of cracks in compositionally modulated two-dimensional semiconductor alloys. *NPJ 2D Mater. Appl.* **2018**, *2*, 10.
123. Wu, S.S.; Huang, T.X.; Xu, X.; Bao, Y.F.; Pei, X.D.; Yao, X.; Cao, M.F.; Lin, K.Q.; Wang, X.; Wang, D.; et al. Quantitatively deciphering electronic properties of defects at atomically thin transition-metal dichalcogenides. *ACS Nano* **2022**, *16*, 4786–4794.
124. Deng, S.; Che, S.; Debbarma, R.; Berry, V. Strain in a single wrinkle on an MoS₂ flake for in-plane realignment of band structure for enhanced photo-response. *Nanoscale* **2019**, *11*, 504–511.
125. Zhang, Y.; Choi, M.-K.; Haugstad, G.; Tadmor, E.B.; Flannigan, D.J. Holey substrate-directed strain patterning in bilayer MoS₂. *ACS Nano* **2021**, *15*, 20253–20260.
126. Martella, C.; Mennucci, C.; Cinquanta, E.; Lamperti, A.; Cappelluti, E.; de Mongeot, F.B.; Molle, A. Anisotropic MoS₂ nanosheets grown on self-organized nanopatterned substrates. *Adv. Mater.* **2017**, *29*, 1605785.
127. Li, H.; Contryman, A.W.; Qian, X.; Ardkani, S.M.; Gong, Y.; Wang, X.; Weisse, J.M.; Lee, C.H.; Zhao, J.; Ajayan, P.M.; et al. Optoelectronic crystal of artificial atoms in strain-textured molybdenum disulphide. *Nat. Commun.* **2015**, *6*, 7381.
128. Li, H.; Du, M.; Mleczko, M.J.; Koh, A.L.; Nishi, Y.; Pop, E.; Bard, A.J.; Zheng, X.L. Kinetic study of hydrogen evolution reaction over strained MoS₂ with sulfur vacancies using scanning electrochemical microscopy. *J. Am. Chem. Soc.* **2016**, *138*, 5123–5129.
129. Wang, S.W.; Medina, H.; Hong, K.B.; Wu, C.C.; Qu, Y.D.; Manikandan, A.; Su, T.Y.; Lee, P.T.; Huang, Z.Q.; Wang, Z.M.; et al. Thermally strained band gap engineering of transition-metal dichalcogenide bilayers with enhanced light matter interaction toward excellent photodetectors. *ACS Nano* **2017**, *11*, 8768–8776.
130. Liu, B.; Liao, Q.; Zhang, X.; Du, J.; Ou, Y.; Xiao, J.; Kang, Z.; Zhang, Z.; Zhang, Y. Strain-engineered van der Waals interfaces of mixed-dimensional heterostructure arrays. *ACS Nano* **2019**, *13*, 9057–9066.
131. Yang, R.; Lee, J.; Ghosh, S.; Tang, H.; Sankaran, R.M.; Zorman, C.A.; Feng, P.X.L. Tuning optical signatures of single- and few-layer MoS₂ by blown-bubble bulge straining up to fracture. *Nano Lett.* **2017**, *17*, 4568–4575.
132. Tyurnina, A.V.; Bandurin, D.A.; Khestanova, E.; Kravets, V.G.; Koperski, M.; Guinea, F.; Grigorenko, A.N.; Geim, A.K.; Grigorieva, I.V. Strained bubbles in van der Waals heterostructures as local emitters of photoluminescence with adjustable wavelength. *ACS Photonics* **2019**, *6*, 516–524.
133. Lloyd, D.; Liu, X.; Christopher, J.W.; Cantley, L.; Wadehra, A.; Kim, B.L.; Goldberg, B.B.; Swan, A.K.; Bunch, J.S. Band gap engineering with ultralarge biaxial strains in suspended monolayer MoS₂. *Nano Lett.* **2016**, *19*, 5836–5841.
134. Manzeli, S.; Allain, A.; Ghadimi, A.; Kis, A. Piezoresistivity and strain-induced band gap tuning in atomically thin MoS₂. *Nano Lett.* **2015**, *15*, 5330–5335.
135. Qi, J.J.; Lan, Y.W.; Stieg, A.Z.; Chen, J.H.; Zhong, Y.L.; Li, L.J.; Chen, C.D.; Zhang, Y.; Wang, K.L. Piezoelectric effect in chemical vapour deposition-grown atomic-monolayer triangular molybdenum disulfide piezotronics. *Nat. Commun.* **2015**, *6*, 7430.
136. Hui, Y.Y.; Liu, X.; Jie, W.; Chan, N.Y.; Hao, J.; Hsu, Y.-T.; Li, L.-J.; Guo, W.; Lau, S.P. Exceptional tunability of band energy in a compressively strained trilayer MoS₂ Sheet. *ACS Nano* **2013**, *7*, 7126–7131.

137. Botello-Méndez, A.R.; López-Urías, F.; Terrones, M.; Terrones, H. Magnetic behavior in zinc oxide zigzag nanoribbons. *Nano Lett.* **2008**, *8*, 1562–1565.
138. Ren, H.; Xiang, G. Morphology-dependent room-temperature ferromagnetism in undoped ZnO nanostructures. *Nanomaterials* **2021**, *11*, 3199.
139. Zhou, J.; Xu, H.; Shi, Y.; Li, J. Terahertz driven reversible topological phase transition of monolayer transition metal dichalcogenides. *Adv. Sci.* **2021**, *8*, 2003832.
140. Enyashin, A.N.; Yadgarov, L.; Houben, L.; Popov, I.; Weidenbach, M.; Tenne, R.; Bar-Sadan, M.; Seifert, G. New route for stabilization of 1T-WS₂ and MoS₂ phases. *J. Phys. Chem. C* **2011**, *115*, 24586–24591.
141. Fuh, H.-R.; Yan, B.; Wu, S.-C.; Felser, C.; Chang, C.-R. Metal-insulator transition and the anomalous Hall effect in the layered magnetic materials VS₂ and VSe₂. *New J. Phys.* **2016**, *18*, 113038.
142. Popov, Z.I.; Mikhaleva, N.S.; Visotin, M.A.; Kuzubov, A.A.; Entani, S.; Naramoto, H.; Sakai, S.; Sorokin, P.B.; Avramov, P.V. The electronic structure and spin states of 2D graphene/VX₂ (X=S, Se) heterostructures. *Phys. Chem. Chem. Phys.* **2016**, *18*, 33047–33052.
143. Yu, W.; Li, J.; Herng, T.S.; Wang, Z.S.; Zhao, X.X.; Chi, X.; Fu, W.; Abdelwahab, I.; Zhou, J.; Dan, J.D.; et al. Chemically exfoliated VSe monolayers with room-temperature ferromagnetism. *Adv. Mater.* **2019**, *31*, 1903779.
144. Zhang, W.; Zhang, L.; Wong, P.K.J.; Yuan, J.R.; Vinai, G.; Torelli, P.; Laan, G.V.D.; Feng, Y.F.; Wee, A.T.S. Magnetic transition in Monolayer VSe interface hybridization. *ACS Nano* **2019**, *13*, 8997–9004.
145. Bonilla, M.; Kolekar, S.; Ma, Y.; Diaz, H.C.; Kalappattil, V.; Das, R.; Eggers, T.; Gutierrez, H.R.; Phan, M.-H.; Batzill, M. Strong room-temperature ferromagnetism in VSe₂ monolayers on van der Waals substrates. *Nat. Nanotechnol.* **2018**, *13*, 289–293.
146. Ataca, C.; Ciraci, S. Functionalization of single-layer MoS₂ honeycomb structures. *J. Phys. Chem. C* **2011**, *115*, 13303–13311.
147. Hong, J.H.; Hu, Z.X.; Probert, M.; Li, K.; Lv, D.H.; Yang, X.N.; Gu, L.; Mao, N.N.; Feng, Q.L.; Xie, L.M.; et al. Exploring atomic defects in molybdenum disulphide monolayers. *Nat. Commun.* **2015**, *6*, 6293.
148. Li, H.; Tsai, C.; Koh, A.L.; Cai, L.L.; Contryman, A.W.; Fragapane, A.H.; Zhao, J.H.; Han, H.S.; Manoharan, H.C.; Abild-Pedersen, F.; et al. Activating and optimizing MoS₂ basal planes for hydrogen evolution through the formation of strained sulphur vacancies. *Nat. Mater.* **2016**, *15*, 48–53.
149. Li, Q.; Zhao, X.; Deng, L.; Shi, Z.; Liu, S.; Wei, Q.; Zhang, L.; Cheng, Y.; Zhang, L.; Lu, H.; et al. Enhanced valley zeeman splitting in Fe-doped monolayer MoS₂. *ACS Nano* **2020**, *14*, 4636–4645.
150. Tan, H.; Hu, W.; Wang, C.; Ma, C.; Duan, H.; Yan, W.; Cai, L.; Guo, P.; Sun, Z.; Liu, Q.; et al. Intrinsic ferromagnetism in Mn-substituted MoS₂ nanosheets achieved by supercritical hydrothermal reaction. *Small* **2017**, *13*, 1701389.
151. Lee, D.; Lee, J.J.; Kim, Y.S.; Kim, Y.H.; Kim, J.C.; Huh, W.; Lee, J.; Park, S.; Jeong, H.Y.; Kim, Y.D.; et al. Remote modulation doping in van der Waals heterostructure transistors. *Nat. Electron.* **2021**, *4*, 664–670.
152. Chen, Y.H.; Tamming, R.R.; Chen, K.; Zhang, Z.; Liu, F.; Zhang, Y.; Hodgkiss, J.M.; Blaikie, R.J.; Ding, B.; Qiu, M. Bandgap control in two-dimensional semiconductors via coherent doping of plasmonic hot electrons. *Nat. Commun.* **2021**, *12*, 4332.
153. Wang, Z.; Xia, H.; Wang, P.; Zhou, X.; Liu, C.; Zhang, Q.; Wang, F.; Huang, M.; Chen, S.; Wu, P.; et al. Controllable doping in 2D layered materials. *Adv. Mater.* **2021**, *33*, 2104942.
154. Zhang, X.; Gao, L.; Yu, H.; Liao, Q.; Kang, Z.; Zhang, Z.; Zhang, Y. Single-atom vacancy doping in two-dimensional transition metal dichalcogenides. *Acc. Mater. Res.* **2021**, *2*, 655–668.
155. Lee, S.J.; Lin, Z.Y.; Duan, X.F.; Huang, Y. Doping on demand in 2D devices. *Nat. Electron.* **2020**, *3*, 77–78.
156. Nethravathi, C.; Prabhu, J.; Lakshmipriya, S.; Rajamathi, M. Magnetic Co-doped MoS₂ nanosheets for efficient catalysis of nitroarene reduction. *ACS Omega* **2017**, *2*, 5891–5897.
157. Shi, X.Y.; Posysaev, S.; Huttula, M.; Pankratov, V.; Hoszowska, J.; Dousse, J.-C.; Zeeshan, F.; Niu, Y.R.; Zakharov, A.; Li, T.H.; et al. Metallic contact between MoS₂ and Ni via Au Nanoglove. *Small* **2018**, *14*, 1704526.
158. Shu, H.B.; Luo, P.F.; Liang, P.; Cao, D.; Chen, X.S. Layer-dependent dopant stability and magnetic exchange coupling of Iron-doped MoS₂ nanosheets. *ACS Appl. Mater. Inter.* **2015**, *7*, 7534–7541.
159. Xiang, Z.; Zhang, Z.; Xu, X.; Zhang, Q.; Wang, Q.; Yuan, C. Room-temperature ferromagnetism in Co doped MoS₂ sheets. *Phys. Chem. Chem. Phys.* **2015**, *17*, 15822–15828.
160. Zhao, Q.; Zhai, C.; Lu, Q.; Zhang, M. Effect of Ho dopant on the ferromagnetic characteristics of MoS₂ nanocrystals. *Phys. Chem. Chem. Phys.* **2019**, *21*, 232–237.
161. Wang, J.; Sun, F.; Yang, S.; Li, Y.; Zhao, C.; Xu, M.; Zhang, Y.; Zeng, H. Robust ferromagnetism in Mn-doped MoS₂ nanostructures. *Appl. Phys. Lett.* **2016**, *109*, 092401.
162. Xia, B.; Guo, Q.; Gao, D.; Shi, S.; Tao, K. High temperature ferromagnetism in Cu-doped MoS₂ nanosheets. *J. Phys. D Appl. Phys.* **2016**, *49*, 165003.
163. Zhang, J.; Lee, W.-K.; Tu, R.; Rhee, D.; Zhao, R.; Wang, X.; Liu, X.; Hu, X.; Zhang, X.; Odom, T.W.; et al. Spontaneous formation of ordered magnetic domains by patterning stress. *Nano Lett.* **2021**, *21*, 5430–5437.
164. Bowden, N.; Brittain, S.; Evans, A.G.; Hutchinson, J.W.; Whitesides, G.M. Spontaneous formation of ordered structures in thin films of metals supported on an elastomeric polymer. *Nature* **1998**, *393*, 146–149.
165. Deng, S.K.; Gao, E.L.; Xu, Z.P.; Berry, V. Adhesion energy of MoS₂ thin films on silicon-based substrates determined via the attributes of a single MoS₂ wrinkle. *ACS Appl. Mater. Inter.* **2017**, *9*, 7812–7818.
166. Santos, E.J.G.; Riikonen, S.; Sánchez-Portal, D.; Ayuela, A. Magnetism of single vacancies in rippled graphene. *J. Phys. Chem. C* **2012**, *116*, 7602–7606.

167. Mohiuddin, T.M.G.; Lombardo, A.; Nair, R.R.; Bonetti, A.; Savini, G.; Jalil, R.; Bonini, N.; Basko, D.M.; Gallois, C.; Marzari, N.; et al. Uniaxial strain in graphene by Raman spectroscopy: G peak splitting, Grüneisen parameters, and sample orientation. *Phys. Rev. B* **2009**, *79*, 205433.
168. He, K.; Poole, C.; Mak, K.F.; Shan, J. Experimental demonstration of continuous electronic structure tuning via strain in atomically thin MoS₂. *Nano Lett.* **2013**, *13*, 2931–2936.
169. Zhu, C.R.; Wang, G.; Liu, B.L.; Marie, X.; Qiao, X.F.; Zhang, X.; Wu, X.X.; Fan, H.; Tan, P.H.; Amand, T.; et al. Strain tuning of optical emission energy and polarization in monolayer and bilayer MoS₂. *Phys. Rev. B* **2013**, *88*, 121301.
170. Yagmurcukardes, M.; Bacaksiz, C.; Unsal, E.; Akbali, B.; Senger, R.T.; Sahin, H. Strain mapping in single-layer two-dimensional crystals via Raman activity. *Phys. Rev. B* **2018**, *97*, 115427.
171. Mak, K.F.; Shan, J.; Ralph, D.C. Probing and controlling magnetic states in 2D layered magnetic materials. *Nat. Rev. Phys.* **2019**, *1*, 646–661.
172. Li, H.; Qi, X.; Wu, J.; Zeng, Z.; Wei, J.; Zhang, H. Investigation of MoS₂ and graphene nanosheets by magnetic force microscopy. *ACS Nano* **2013**, *7*, 2842–2849.
173. Yang, S.; Wang, C.; Sahin, H.; Chen, H.; Li, Y.; Li, S.-S.; Suslu, A.; Peeters, F.M.; Liu, Q.; Li, J.; et al. Tuning the optical, magnetic, and electrical properties of ReSe₂ by nanoscale strain engineering. *Nano Lett.* **2015**, *15*, 1660–1666.
174. Schmid, I.; Marioni, M.A.; Kappenberger, P.; Romer, S.; Parlinska-Wojtan, M.; Hug, H.J.; Hellwig, O.; Carey, M.J.; Fullerton, E.E. Exchange bias and domain evolution at 10 nm scales. *Phys. Rev. Lett.* **2010**, *105*, 197201.
175. Moser, A.; Xiao, M.; Kappenberger, P.; Takano, K.; Weresin, W.; Ikeda, Y.; Do, H.; Hug, H.J. High-resolution magnetic force microscopy study of high-density transitions in perpendicular recording media. *J. Magn. Magn. Mater.* **2005**, *287*, 298–302.
176. Mattiat, H.; Rossi, N.; Gross, B.; Pablo-Navarro, J.; Magén, C.; Badea, R.; Berezhovsky, J.; De Teresa, J.M.; Poggio, M. Nanowire magnetic force sensors fabricated by focused-electron-beam-induced deposition. *Phys. Rev. Appl.* **2020**, *13*, 044043.
177. Jeffery, M.; Van Duzer, T.; Kirtley, J.R.; Ketchen, M.B. Magnetic imaging of moat-guarded superconducting electronic circuits. *Appl. Phys. Lett.* **1995**, *67*, 1769–1771.
178. Sheng, Z.; Feng, Q.; Zhou, H.; Dong, S.; Xu, X.; Cheng, L.; Liu, C.; Hou, Y.; Meng, W.; Sun, Y.; et al. Visualization of electronic multiple ordering and its dynamics in high magnetic field: evidence of electronic multiple ordering crystals. *ACS Appl. Mater. Inter.* **2018**, *10*, 20136–20141.
179. Kirtley, J.R.; Paulius, L.; Rosenberg, A.J.; Palmstrom, J.C.; Holland, C.M.; Spanton, E.M.; Schiessl, D.; Jermain, C.L.; Gibbons, J.; Fung, Y.K.K.; et al. Scanning SQUID susceptrometers with sub-micron spatial resolution. *Rev. Sci. Instrum.* **2016**, *87*, 093702.
180. Vasyukov, D.; Anahory, Y.; Embo, L.; Halbertal, D.; Cuppens, J.; Neeman, L.; Finkler, A.; Segev, Y.; Myasoedov, Y.; Rappaport, M.L.; et al. A scanning superconducting quantum interference device with single electron spin sensitivity. *Nat. Nanotechnol.* **2013**, *8*, 639–644.
181. Gong, C.; Li, L.; Li, Z.L.; Ji, H.W.; Stern, A.; Xia, Y.; Cao, T.; Bao, W.; Wang, C.Z.; Wang, Y.A.; et al. Discovery of intrinsic ferromagnetism in two-dimensional van der Waals crystals. *Nature* **2017**, *546*, 265–269.
182. Huang, B.; Clark, G.; Navarro-Moratalla, E.; Klein, D.R.; Cheng, R.; Seyler, K.L.; Zhong, D.; Schmidgall, E.; McGuire, M.A.; Cobden, D.H.; et al. Layer-dependent ferromagnetism in a van der Waals crystal down to the monolayer limit. *Nature* **2017**, *546*, 270.
183. Thiel, L.; Wang, Z.; Tschudin, M.A.; Rohner, D.; Gutiérrez-Lezama, I.; Ubrig, N.; Gibertini, M.; Giannini, E.; Morpurgo, A.F.; Maletinsky, P. Probing magnetism in 2D materials at the nanoscale with single-spin microscopy. *Science* **2019**, *364*, 973–976.
184. Chang, K.; Eichler, A.; Rhensius, J.; Lorenzelli, L.; Degen, C.L. Nanoscale imaging of current density with a single-spin magnetometer. *Nano Lett.* **2017**, *17*, 2367–2373.
185. Wörnle, M.S.; Welter, P.; Giraldo, M.; Lottermoser, T.; Fiebig, M.; Gambardella, P.; Degen, C.L. Coexistence of Bloch and N'eel walls in a collinear antiferromagnet. *Phys. Rev. B* **2021**, *103*, 094426.
186. Ariyaratne, A.; Bluvstein, D.; Myers, B.A.; Jayich, A.C.B. Nanoscale electrical conductivity imaging using a nitrogen-vacancy center in diamond. *Nat. Commun.* **2018**, *9*, 2406.
187. Vool, U.; Hamo, A.; Varnavides, G.; Wang, Y.; Zhou, T.X.; Kumar, N.; Dovzhenko, Y.; Qiu, Z.; Garcia, C.A.C.; Pierce, A.T.; et al. Imaging phonon-mediated hydrodynamic flow in WTe₂. *Nat. Phys.* **2021**, *17*, 1216–1220.
188. Wang, J.; Luo, Y.; Cai, X.; Shi, R.; Wang, W.; Li, T.; Wu, Z.; Zhang, X.; Peng, O.; Amini, A.; et al. Multiple regulation over growth direction, band structure, and dimension of monolayer WS₂ by a quartz substrate. *Chem. Mater.* **2020**, *32*, 2508–2517.
189. Rasaili, P.; Sharma, N.K.; Bhattacharai, A. Comparison of ferromagnetic materials: past work, recent trends, and applications. *Condens. Matter* **2022**, *7*, 12.
190. Li, H.; Ruan, S.C.; Zeng, Y.J. Intrinsic van der Waals magnetic materials from bulk to the 2D limit: new frontiers of spintronics. *Adv. Mater.* **2019**, *31*, 1900065.
191. Li, X.X.; Dong, B.J.; Sun, X.D.; Wang, H.W.; Yang, T.; Yu, G.Q.; Han, Z.V. Perspectives on exfoliated two-dimensional spintronics. *J. Semi.* **2019**, *40*, 081508.
192. Guo, Y.L.; Wang, B.; Zhang, X.W.; Yuan, S.J.; Ma, L.; Wang, J.L. Magnetic two-dimensional layered crystals meet with ferromagnetic semiconductors. *InfoMat* **2020**, *2*, 639–655.
193. Liu, Y.P.; Zeng, C.; Zhong, J.H.; Ding, J.N.; Wang, Z.M.; Liu, Z.W. Spintronics in two-dimensional materials. *Nano-Micro Lett.* **2020**, *12*, 93.
194. Xu, J.J.; Li, W.; Hou, Y.L. Two-dimensional magnetic nanostructures. *Trends in Chem.* **2020**, *2*, 163–173.
195. Jiang, X.; Liu, Q.X.; Xing, J.P.; Liu, N.S.; Guo, Y.; Liu, Z.F.; Zhao, J.J. Recent progress on 2D magnets: fundamental mechanism, structural design and modification. *Appl. Phys. Rev.* **2021**, *8*, 031305.

196. Zhang, S.F.; Wu, H.; Yang, L.; Zhang, G.J.; Xie, Y.M.; Zhang, L.; Zhang, W.F.; Chang, H.X. Two-dimensional magnetic atomic crystals. *Mater. Horiz.* **2021**, *9*, 559–576.
197. Hossain, M.; Qin, B.; Li, B.; Duan, X.D. Synthesis, characterization, properties and applications of two-dimensional magnetic materials. *Nano Today* **2022**, *42*, 101338.
198. Wang, Y.; Wang, C.; Liang, S.J.; Ma, Z.; Xu, K.; Liu, X.; Zhang, L.; Admasu, A.S.; Cheong, S.-W.; Wang, L.; et al. Strain-sensitive magnetization reversal of a van der Waals magnet. *Adv. Mater.* **2020**, *32*, 2004533.
199. Miao, F.; Liang, S.J.; Cheng, B. Straintronics with van der Waals materials. *NPJ Quantum Mater.* **2021**, *6*, 59.
200. Yan, Y.L.; Ding, S.; Wu, X.N.; Zhu, J.; Feng, D.M.; Yang, X.D.; Li, F.F. Tuning the physical properties of ultrathin transition-metal dichalcogenides via strain engineering. *RSC Adv.* **2020**, *10*, 39455–39467.
201. Zhao, Z.Y.; Liu, K.; Liu, Y.W.; Guo, Y.L.; Liu, Y.Q. Intrinsically flexible displays: key materials and devices. *Natl. Sci. Rev.* **2022**, *10.1093/nsr/nwac090*
202. Liu, R.Y.; Wang, Z.L.; Fukuda, K.; Someya, T. Flexible self-charging power sources. *Nat. Rev. Mater.* **2022**, *1*–17. <https://doi.org/10.1038/s41578-022-00441-0>.